Studies on the Decay and Recovery of Higher-Order Solitons, Initiated by Localized Channel Perturbations

A Thesis
Presented to
The Academic Faculty

by

Kwan-Seop Lee

In Partial Fulfillment
of the Requirement for the Degree of
Doctor of Philosophy
in Electrical Engineering

Georgia Institute of Technology
March 2004

To my wife, Yun-Jeong

Acknowledgements

I would like to first thank Dr. John Buck. He has been a good advisor throughout my entire doctoral program. He always encouraged me with extreme patience. I strongly appreciate him for his guidance and support.

I appreciate the members of my reading committee, Dr. Stephen Ralph and Dr. Gee-Kung Chang for their advices about my thesis. I would also like to thank the other members of my committee, Dr. Glenn Smith and Dr. Rick Trebino. I would like to thank Ultrafast Optics Laboratory for allowing me to access their equipments and facilities. I am grateful to Michael Gross, Ketan Patel, Jeffrey Lillie, Arup Polley, and Jung Lee for their help with my experimental studies.

I would like to thank my family. I thank my mother for her constant love, and my father for his advice and encouragement. I thank my two sons, Daniel and David, who always make me happy and make me learn many things in my life.

Finally, I would like to give my deepest appreciation to my wife, Yun-Jeong, for being with me. Her consistent love enabled me to complete this work.

Table of Contents

List of Terms

SSFM Split-Step Fourier Method

NLSE Non-Linear Schödinger Equation

MNLSE Modified Non-Linear Schödinger Equation

ASE Amplified Spontaneous Emission

GVD Group-Velocity Dispersion

SPM Self-Phase Modulation

OSA Optical Spectrum Analyzer

EDFA Erbium-Doped Fiber Amplifier

LDF Low Dispersion Fiber

HDF High Dispersion Fiber

NDF Negative Dispersion Fiber

DCF Dispersion Compensating Fiber

MFD Mode Field Diameter

List of Figures

Summary

The decay of higher order solitons in optical fiber, initiated by localized channel perturbations such as a step change in dispersion, a localized loss element, or a bandpass filter, is explored theoretically and experimentally as a means of generating pairs of pulses having wavelengths that are up and down-shifted from the input wavelength. The achievable wavelength separation between the two sub pulses increases with increasing the amount of perturbations. Pulse parameter requirements for achieving useful wavelength shifts while avoiding unwanted nonlinear effects are presented.

Experimental studies for N=2 solitons having 1 ps initial width are performed to demonstrate tunable wavelength conversion using a step change in dispersion and using a loss element. Wavelength shifts are tunable by varying the magnitude of a dispersion step or loss element that is used to disrupt the soliton cycle. Competing nonlinear effects, such as cubic dispersion, self-steepening, and stimulated Raman scattering, can be minimized by using input pulsewidths of one picosecond or greater. The separated pulses at two wavelengths can in principle be amplified to form separate higher order solitons. The process repeated to produce multiple wavelength replicas of an input data stream, and may thus be of possible use in multi-casting applications in fiber communication systems.

The possibility of soliton recovery is also studied. For soliton recovery, conditions are stringent, in that the precise temporal overlap and phase relationship between sub-pulses that occurred at the point of separation is in principle needed at the reverse perturbation location. Experimental studies on soliton recovery for an N=2 soliton is performed by using a dispersion-compensated intermediate link, and reversing the dispersion step. Detrimental effects on soliton recovery are studied.

CHAPTER 1

INTRODUCTION

1.1 Research Motivation and Objectives

The decay of higher-order solitons to form sub-pulses in optical fiber has been reported in early work to arise from phenomena such as self-steepening [1]-[2], stimulated Raman scattering [3], cubic dispersion in the vicinity of the zero dispersion wavelength [4], and in transitioning between negative and positive dispersion in dispersion-increasing fiber [5]. A recent theoretical study demonstrated the feasibility of using localized channel perturbations to initiate higher-order soliton decay [6]-[7]. During higher-order soliton decay, shifted-wavelength sub-pulses are formed in optical fiber. This property is useful for wavelength conversion applications.

We propose a novel wavelength conversion method through N=2 or N=3 soliton decay, initiated by any one of three forms of localized perturbations in the fiber channel. These include 1) a step increase in dispersion, 2) a loss element, or 3) a bandpass filter. All result in the conversion of the soliton into two sub-pulses at wavelengths that are up and down shifted from that of the input pulse. The wavelengths can be varied by adjusting the magnitude of the perturbation. In principle, the converted pulses can be

amplified to form new higher order solitons, and the process repeated to produce multiple wavelengths of variable spacing. The converted pulses may form into fundamental solitons, or may propagate in the linear regime, depending on the perturbation conditions. In the case of linear sub-pulse propagation, we have found that the process can be reversed – in that the separated pulses at two wavelengths can be recombined to restore the higher order soliton at the original wavelength by using a reverse perturbation down-channel.

We envision the wavelength conversion as a method of replicating RZ data, forming duplicate data streams at two or more wavelengths that are shifted from the original wavelength. In one part of the proposed work, we intend to explore multicasting applications using the effect. We envision the pulse recovery process as having applications to secure data transmission, as will be discussed. Of specific interest at the physical layer are the required configurations of optical amplifiers and filters such that stable data streams at multiple wavelengths can be successfully generated from a single wavelength source, and then separated using standard WDM filters for distribution to multiple subscribers. Conditions for fundamental soliton generation at the multiple wavelengths are to be determined, as well as allowed tolerances in power levels and in link parameters. For soliton recovery, conditions are stringent, in that the precise temporal overlap and phase relationship between sub-pulses that occurred at the point of separation is in principle needed at the reverse perturbation location. Our numerical results and experiments have shown that some departure from the ideal conditions is

tolerable, which leads us to conclude that the process requires further investigation. A method of secure data transmission, based on the recovery concept, is proposed.

The object of this research is to investigate the decay and recovery of higher-order solitons initiated by localized channel perturbations. A detailed modeling effort for soliton propagation in optical fibers is performed to accomplish this task. A simulation tool is developed using the split step Fourier method (SSFM). Higher-order soliton decay, initiated by a localized channel perturbation in the fiber channel, is demonstrated theoretically and experimentally as a means of generating pairs of pulses having wavelengths that are up and down-shifted from the input wavelength. The amount of wavelength shift is tunable by controlling the magnitude of the perturbation. Pulse parameter requirements for achieving useful wavelength shifts while avoiding unwanted nonlinear effects are presented. Experimental works for N=2 solitons having 1 ps initial width are performed to demonstrate tunable wavelength conversion using a step change in dispersion and using a loss element. The separated pulses at two wavelengths can in principle be amplified to form separate higher order solitons. The process repeated to produce multiple wavelength replicas of an input data stream, and may thus be of possible use in multi-casting applications in fiber communication systems.

The possibility of soliton recovery is also studied. The conditions are described, under which the separated pulses can be re-combined at a distant location to restore the higher order soliton at the original wavelength. Experiments on soliton recovery using a dispersion-compensated intermediate link and reversing the dispersion step will be performed to verify the theoretical predictions.

1.2 Higher-Order Soliton Decay

Golovchenko et al. have reported the decay of femtosecond higher-order solitons in an optical fiber [1]. They found that the higher-order solitons are structurally unstable, and that a perturbation in the modified non-linear Schödinger equation (MNLSE) could cause remarkable changes in the nonlinear dynamics of intense sub-picosecond pulses. Among their other results, they found that the effect of self-steepening leads to breakup of higher-order solitons into their constituents or sub-solitons. A second-order soliton (N=2) breaks up into two solitons, which have separated from each other within several soliton periods. Third-order solitons (N=3) show a similar decay patterns, and decay into three pulses [2].

The inverse scattering method with perturbation theory is helpful in understanding the soliton decay [8]-[9]. Solitons form a bound state when no perturbation exists. They have the same group velocity because their eigenvalues have the same real part. The effect of a perturbation is to introduce an instability into the bound state of solitons and to decrease the lifetime of the bound states. As a result, the degeneracy is broken. Two solitons have different group velocities and propagate at different speeds. They move apart each other and then separate asymptotically.

C. R. Menyuk reported that solitons are robust in the presence of Hamiltonian (energy preserving) perturbations such as dispersion and birefringence but are destroyed in the presence of non-Hamiltonian (energy lost) perturbations such as attenuation, filtering, and the Raman effect because soliton solutions do not exist with non-Hamiltonian perturbations [10]. However, higher-order solitons can be destroyed in the

presence of Hamiltonian perturbation when the amount of perturbation exceeds a threshold value.

Kuochou Tai and Akira Hasegawa show the decay process induced by the stimulated Raman effect using a contour plot of pulse trajectory for N=2 and N=3 [3]. The decay pattern is similar to the case of self-steepening. The second-order soliton breaks up into two pulses and the third-order soliton decays into three pulses. The difference is that one soliton is advanced and the others are delayed in the case of the Raman effect, while all the solitons are delayed in the case of self-steepening. Hodel and Weber demonstrated that the Raman effect dominates the shock term on femtosecond time scales and leads to the decay of higher-order solitons [11]. After the decay of higher-order solitons, each constituent shapes into a soliton-like pulse.

Previous studies of the decay of higher-order solitons are applicable on a femtosecond time scale. In our study, we describe the decay of a higher-order soliton on a picosecond time scale by using different kinds of perturbations. These include attenuation, filtering, and a dispersion change using a short length of dispersion-shifted fiber. Higher-order solitons are broken into their constituent pulses within several soliton periods when they are perturbed by a loss element, band-pass filter, or a dispersion change at the propagation location, at which their spectral bandwidths are at a maximum. After the decay of higher-order solitons, each constituent shapes into a soliton-like pulse. A second-order soliton (N=2) splits into two solitons. These continue to move apart with further propagation and then separate asymptotically inside the fiber. Two solitons have almost zero chirps and have center wavelengths that are different from that of the original

pulse; the new wavelength values are below and above that of the original pulse. Using the higher-order soliton decay, it is possible to generate two copies of an optical data stream, in which the copies are at different wavelengths. These wavelengths are also different from that of the original data. The data copies can be amplified and the process repeated to achieve multiple copies. Our method is very simple and in principle error-free.

1.3 Research Overview

The goal of this research is to investigate the higher-order soliton decay process initiated by localized channel perturbations. A detailed modeling effort is performed to accomplish this task. The applications of soliton decay will be proposed. The important steps for the research are described below.

This thesis is divided into five remaining chapters. Chapter 2 describes soliton propagation in optical fibers. A detailed modeling effort for this is performed. We solve the non-linear Schödinger equation (NLSE) using the split-step Fourier method (SSFM). Numerical studies are done for N=1, N=2, and N=3 soliton propagation.

In Chapter 3, higher-order soliton decay will be studied. Numerical studies will be performed for N=2 and N=3 soliton decay initiated by localized channel perturbations. Pulse parameter requirements for achieving useful wavelength shifts while avoiding unwanted nonlinear effects are presented. Tunable wavelength separation is presented by controlling the magnitude of the perturbation.

Chapter 4 proposes a tunable wavelength conversion method using N=2 soliton decay initiated by step changes in dispersion. We demonstrate wavelength conversion theoretically and experimentally.

In Chapter 5, the possibility of soliton recovery is studied. The conditions are described, under which the separated pulses can be re-combined at a distant location to restore the higher order soliton at the original wavelength. We demonstrate soliton recovery numerically and experimentally.

Applications will be proposed in Chapter 6. These include multicasting using multi-wavelength data replication, and secure data transmission using the phase-sensitive properties of soliton recovery. The conclusion of this research is summarized in Chapter 7.

CHAPTER 2

SOLITON PROPAGATION IN OPTICAL FIBERS

2.1 Introduction

In this chapter, we study soliton propagation in optical fibers. A numerical model will be developed to describe the soliton propagation. The nonlinear Schrödinger equation (NLSE), modified to include cubic dispersion, self-steepening, and stimulated Raman scattering, will be solved numerically using the Split-Step Fourier Method (SSFM). Numerical results will be presented for N=1, N=2, and N=3 soliton propagation.

2.2 Numerical Analysis

The nonlinear Schrodinger equation (NLSE) is a basic equation for the description of pulse propagation in optical fibers that are nonlinear and dispersive. The NLSE can be derived from the wave equation after the effects of the nonlinearity and dispersion are included under the slowly-varying envelope approximation. The derivation of the NLSE from wave equation can be found in Chapter 7 of the reference [12]. The resulting NLSE, modified to include higher-order effects, is:

$$\frac{\partial A}{\partial z}+\frac{1}{v_g}\frac{\partial A}{\partial t}+\frac{i}{2}\beta_2\frac{\partial^2 A}{\partial t^2}+\frac{\alpha}{2}A=i\gamma|A|^2A+\frac{1}{6}\beta_3\frac{\partial^3 A^2}{\partial t^3}-\frac{\gamma}{\omega_0}\frac{\partial}{\partial t}\left(|A|^2A\right)-i\gamma T_R\frac{\partial|A|^2}{\partial t}A, \tag{2.2.1}$$

where A is the complex envelope of the pulse, z is the propagation distance, t is the time, v_g is the group velocity, β_2 is the quadratic dispersion coefficient, β_3 is the cubic dispersion coefficient, α is the fiber loss, T_R is the Raman response parameter, and $\gamma = \omega_0 n_2 / (c A_{eff})$ is the nonlinear parameter at the carrier angular frequency ω_0. A_{eff} is the effective core area of the fiber.

This equation is valid for describing the propagation of pulses as short as ~ 50 fs. The last three terms embody the higher-order effects; they are, respectively, cubic dispersion, self-steepening, and stimulated Raman scattering. The effect of cubic dispersion becomes important for ultrashort pulses, whose bandwidths are large. Under such conditions, cubic dispersion is important even when the wavelength λ is relatively far away from the zero-dispersion wavelength λ_0 [13]-[14]. The effect of self-steepening

is responsible for shock formation at a pulse edge [15]-[17]. The last term, proportional to T_R, results from Stimulated Raman scattering, and is responsible for the self-frequency shift, which transfers energy from shorter-wavelengths to longer-wavelengths.

It is convenient to use normalized dimensionless units by using the definitions

$$U = \frac{A}{\sqrt{P_0}}, \tag{2.2.2}$$

$$\xi = \frac{z}{L_D}. \tag{2.2.3}$$

$$\tau = \frac{t - z/v_g}{T_0}, \tag{2.2.4}$$

In the equation, U is the complex envelope of the pulse normalized to the initial pulse peak power P_0, ξ is the distance normalized to the dispersion length L_D, and τ is the local time (measured from the pulse center) normalized with respect to the characteristic width T_0 of the hyperbolic secant pulse. T_0 is related to the full-width at half-maximum intensity of the input pulse through $\Delta T_f = 1.763\ T_0$. The dispersion distance L_D is defined as

$$L_D = \frac{T_0^{\,2}}{|\beta_2|}. \tag{2.2.5}$$

The pulse is assumed to propagate in the region of anomalous group velocity dispersion ($\beta_2<0$) and the fiber loss is neglected ($\alpha=0$). Using Equations (2.2.2) ~ (2.2.4), Equation (2.2.1) is transformed to the normalized from:

$$\frac{\partial U}{\partial z} - \frac{i}{2}\frac{\partial^2 U}{\partial \tau^2} - \delta\frac{\partial^3 U}{\partial \tau^3} = iN^2\left[|U|^2 U + is\frac{\partial}{\partial \tau}(|U|^2 U) - \tau_R U\frac{\partial}{\partial \tau}(|U|^2)\right]. \tag{2.2.6}$$

The cubic dispersion, self-steepening, and Raman response parameters are respectively given by $\delta=\beta_3/(6|\beta_2|T_0)$, $s=1/(T_0\omega_0)$, and $\tau_R=T_R/T_0$, where T_R = 3 fs [18]. The soliton order N in Equation (2.2.6) can be expressed in the form:

$$N = \left[\frac{4cn_2}{\lambda^3|D(\lambda)|A_{eff}}\right]^{1/2}\left[1.8\Delta T_f\sqrt{P_0}\right], \qquad (2.2.7)$$

where n_2 is the nonlinear refractive index, A_{eff} is the effective area of the fiber mode intensity, and $D(\lambda)$ is the quadratic dispersion in ps/nm-km. N provides a measure of the strength of the nonlinear response compared to the fiber dispersion. Not only the initial pulse width T_0 and the peak power P_0 of the incident pulse, but also the fiber parameters n_2, A_{eff}, and D can change the soliton order N.

The effects of δ, s, and τ_R are described in detail later. To minimize their contributions, pulses must be sufficiently broad to enable modest peak powers and longer rise and fall times, while satisfying the higher order soliton condition. Consequently, we are constrained to input pulses of widths T_0>1ps such that $T_0\omega_0$>>1 and T_R/T_0<<1, at which δ, s, and τ_R can be negligible [19]. For pulse widths of the order of 1 ps or longer, Equation (2.2.6) can be simplified to the following:

$$\frac{\partial U}{\partial \tau}+\frac{i}{2}\frac{\partial^2 U}{\partial \tau^2}=iN^2|U|^2U\,. \qquad (2.2.8)$$

Equation (2.2.8) is referred to as the NLSE and has been extensively studied in the context of solitons, which are its solutions. Optical solitons can exist through balance and interplay between the dispersive (GVD) and nonlinear (SPM) properties of optical fibers. Fundamental solitons correspond to the case of a single eigenvalue (N=1). They can

propagate over arbitrarily long distances, maintaining their shapes and widths in time and in the spectral domain. Fundamental solitons are a good candidate for high-speed data transmission systems because they can easily overcome GVD induced pulse broadening.

Higher-order solitons are the general solutions of the NLSE for integer values of N greater than 1. Instead of propagation without changing shape, they show periodic propagation behavior in their shapes and widths over the soliton period, $z_0 = \frac{\pi}{2} L_D$. Higher-order solitons have found applications to optical pulse compression.

To investigate soliton propagation in optical fibers, we numerically solved Equation (2.2.8) using the Split-step Fourier method, which will be introduced in the next section.

2.3 Numerical Method: Split-step Fourier Method

NLSE can be written using to operators $\hat{D}$ and $\hat{N}$ in the form [19]

$$\frac{\partial A}{\partial z} = (\hat{D} + \hat{N})A, \tag{2.3.1}$$

where $\hat{D}$ is a linear operator and $\hat{N}$ is a nonlinear operator. These operators are given by

$$\hat{D} = -\frac{i}{2}\frac{\partial^2}{\partial \tau^2} - \delta\frac{\partial^3}{\partial \tau^3} \tag{2.3.2}$$

$$\hat{N} = iN^2\left[|U|^2 U + is\frac{\partial}{\partial \tau}(|U|^2 U) - \tau_R U\frac{\partial}{\partial \tau}(|U|^2)\right]. \tag{2.3.3}$$

The operator $\hat{D}$ includes the effects of dispersion in a linear medium, whereas the operator $\hat{N}$ includes the effects of fiber nonlinearities on pulse propagation. During the pulse propagation, dispersion and nonlinearity act together. This makes the numerical solution complicated. Under some assumption that dispersion and nonlinearity can act independently during the propagation of the optical field over a small distance, the numerical solution can be easily obtained. The split-step Fourier method adopts this assumption for the independent actions of GVD and SPM to obtain an approximate numerical solution. For example, propagation from z to z+h is carried out in two steps. In the first step, only nonlinearity is considered by setting $\hat{D}$=0. In the second step, only dispersion is considered by setting $\hat{N}$ = 0. This can be expressed mathematically

$$A(z+h,T) = \exp(h\hat{D})\exp(h\hat{N})A(z,T). \tag{2.3.4}$$

The SSFM uses the Fourier-transform operation to carry out the exponential operator $\exp(h\hat{D})$ in the Fourier domain using the relation

$$\exp(h\hat{D})B(z,T) = \{F^{-1}\exp[h\hat{D}(w)]F\}B(z,T), \qquad (2.3.5)$$

where F is the Fourier-transform operation and $\hat{D}(w)$ is a Fourier-transform of Equation (2.3.2), which can be obtained by replacing the differential operator $\frac{\partial}{\partial T}$ by $i\omega$ in the equation. The use of the FFT algorithm can make numerical evaluation of Equation (2.3.5) relatively fast comparing to other numerical methods.

FIGURE 2.1 shows an operation diagram of the symmetrized split-step Fourier method used for numerical simulations. The propagation path is partitioned into a number of segments. The step size h should be small enough to satisfy the accuracy requirement for the approximation. As the step size decreases, accuracy increases but computation time is also increases. First, GVD acts alone in frequency domain without SPM between the input and the center of each segment. At the center of the segment, SPM is considered in time domain without GVD. Then GVD acts alone again in frequency domain without SPM through the remaining half of the segment. This process is repeated until all segments are completed.

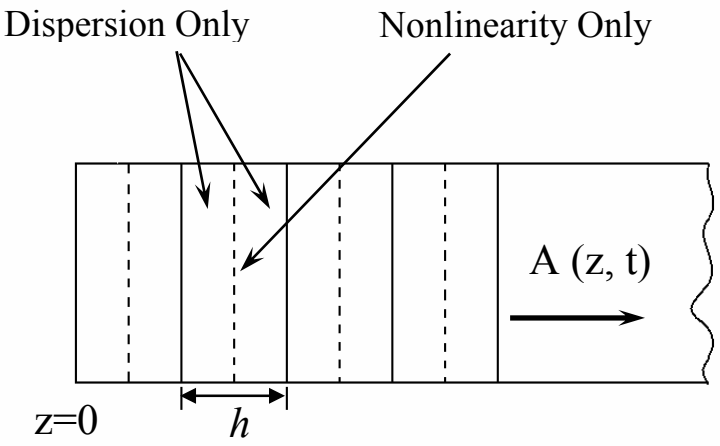

FIGURE 2.1 Operation diagram of the split-step Fourier method used for numerical simulations [19].

2.4 Numerical Results

To investigate soliton propagation in optical fibers, we numerically solved the NLSE using Split-step Fourier method with the initial envelope of the soliton at $\xi = 0$ given by $U(0,\tau)=\text{sech}(\tau)$ for N=1, N=2, and N=3 cases.

2.4.1 Fundamental soliton propagation (N=1)

Figures 2.2a and b show the temporal and spectral evolution of a fundamental soliton over one soliton period z_0, where the latter is given by $z_0 = \frac{\pi}{2} L_D$. It shows that the soliton can propagate with an unchanging pulse envelope and its spectrum over long distances. This can be achieved through the balance between the effects of SPM and GVD.

The physical process of a fundamental soliton propagation can be explained by considering the effects of SPM and GVD. During the pulse evolution, the effect of SPM is to produce positive chirp, whereas the effect of GVD (D>0) is to produce negative chirp. When relative strengths of SPM and GVD are exactly balanced, positive chirp generated by SPM is completely cancelled out by negative chirp generated by GVD. As a result, the pulse exhibits a zero chirp with time over its entire width. Under this condition, the pulse propagates without broadening or compressing for long distances.

The soliton order, N, is an indicator of nonlinear strength, which means the ratio of the strength of nonlinear effect to that of dispersion effect. For fundamental solitons (N=1), the effects of SPM and GVD are exactly balanced.

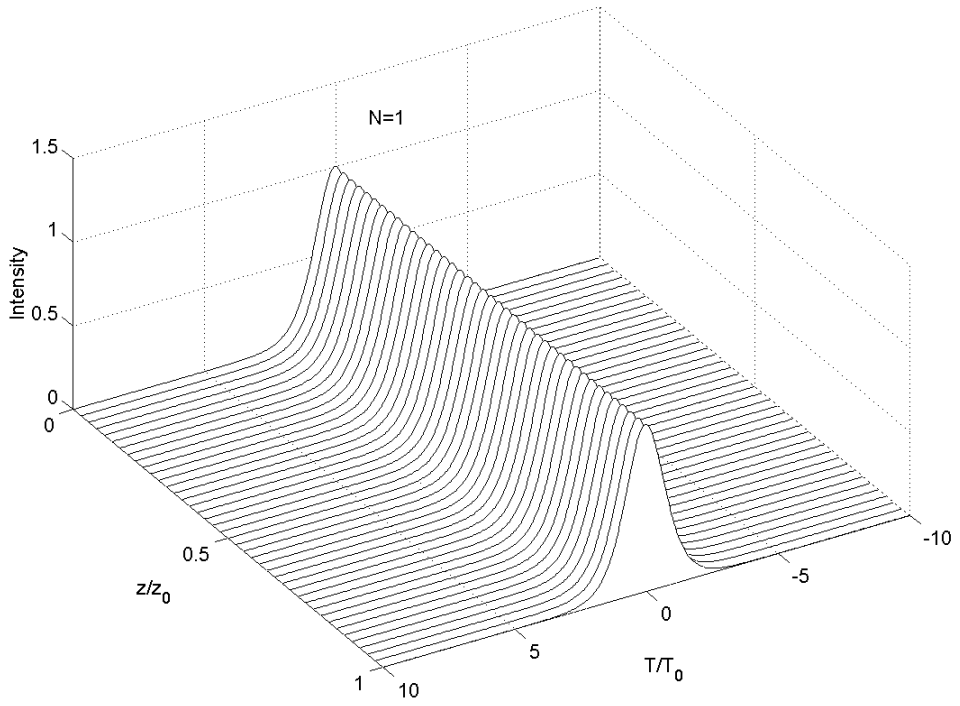

FIGURE 2.2a Temporal evolution of an N=1 soliton over one soliton period, z_0. The intensity is normalized to the input peak intensity.

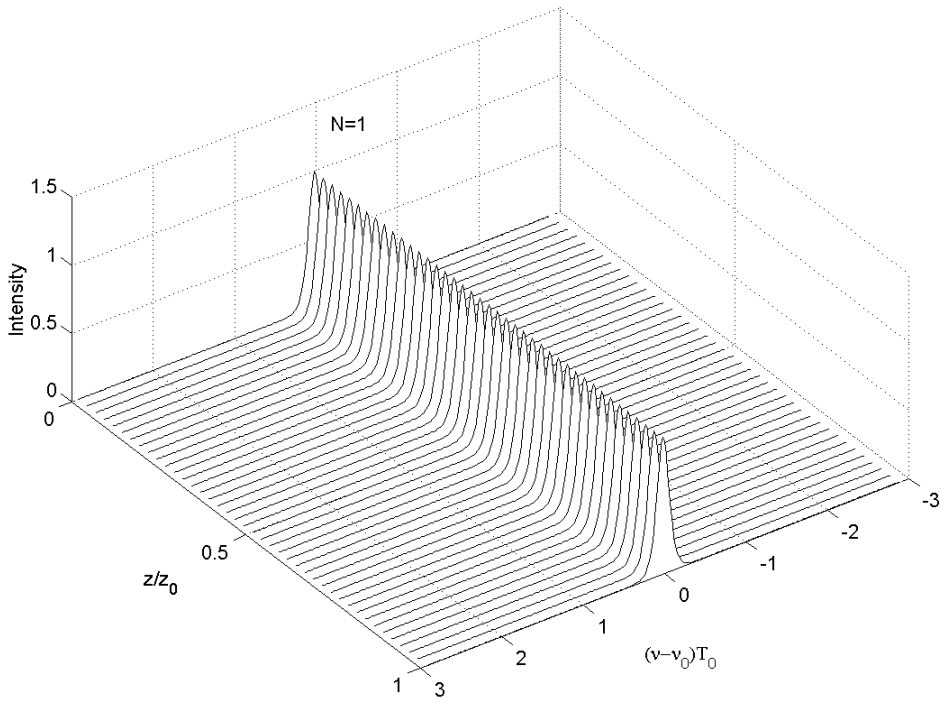

FIGURE 2.2b Spectral evolution of an N=1 soliton over one soliton period, z_0. The intensity is normalized to the input peak intensity.

2.4.2 Second-order soliton propagation (N=2)

If *N* is an integer greater than 1, pulse evolution is totally different from the case of a fundamental soliton. Evolution of this *N*th-order soliton is periodic. For higher-order solitons, the effect of SPM dominates the effect of GVD (N>1). As discussed in the previous section, the effect of SPM is to produce positive chirp, whereas the effect of GVD (D>0) is to produce negative chirp. Because of the higher intensity, the amount of positive chirp generated by SPM is greater than that of negative chirp produced by GVD; it cannot be cancelled out completely. As a result, the pulse acquires positive chirp.

The effect of GVD (D>0) for a positively chirped pulse is to compress the pulse by forcing the energies associated with its spectral components toward the center. With SPM of greater magnitude than in the N =1 case, the pulse would compress until the energies reach the center. As they pass through the center, the pulse will broaden again.

The temporal and spectral evolution of an N =2 soliton are shown in Figures 2.3a and b. In time domain, the pulse compresses up to the distance $z_0/2$, at which it has a minimum pulse width. This pulse compression occurs because N is greater than 1. The amount of positive chirp from SPM is too large to be canceled by negative chirp generated from GVD. As a result, it is accumulated and is increased up to the distance $z_0/2$, where the shifted energies by positive dispersion coincide at the pulse center. As soon as they pass through the center, the sign of chirp is changed from positive to negative. The effect of GVD (D>0) for a negatively chirped-pulse is to broaden the pulse. After the distance $z_0/2$, the pulse begins to re-broaden. Because positive chirp generated by SPM rapidly cancels the negative chirp on the pulse, the amount of negative chirp is

decreased and pulse spreading slows down. The chirp becomes zero at the distance z_0, where the pulse stabilizes at its original width. The process then repeats.

In spectral domain, the pulse spectrum broadens as the pulse compression occurs. At the distance $z_0/2$, the spectrum splits to form two peaks. This can be interpreted as two overlapping pulses at the two wavelengths in time domain. After the distance $z_0/2$, the separated spectral peaks recombine as the pulse propagates. Then the spectrum is recompressed to recover the original input spectrum.

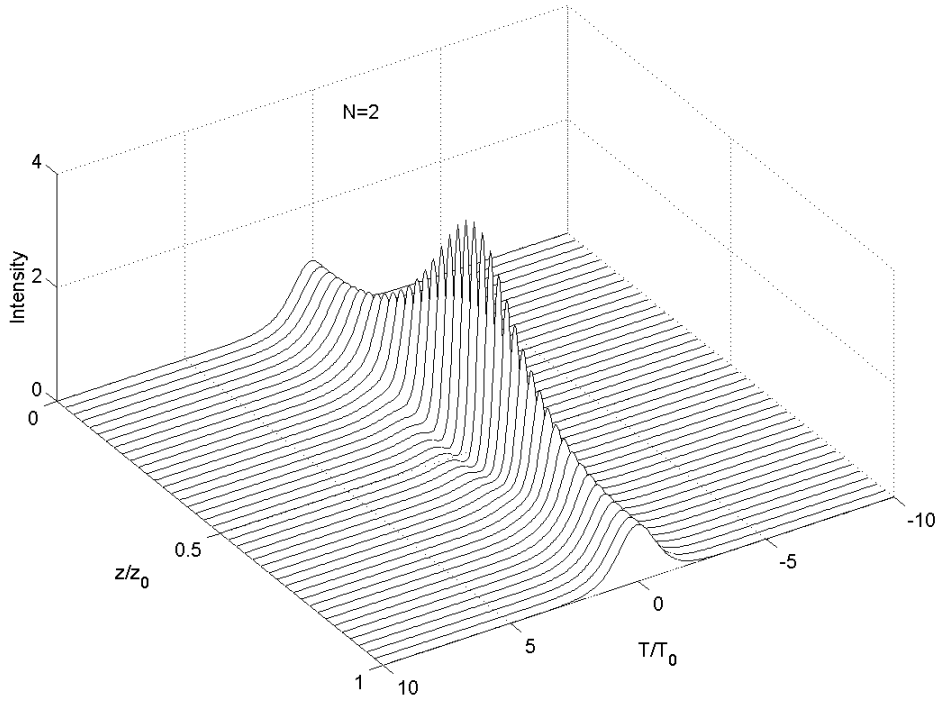

FIGURE 2.3a Temporal evolution of an N=2 soliton over one soliton period, z_0. The intensity is normalized to the input peak intensity.

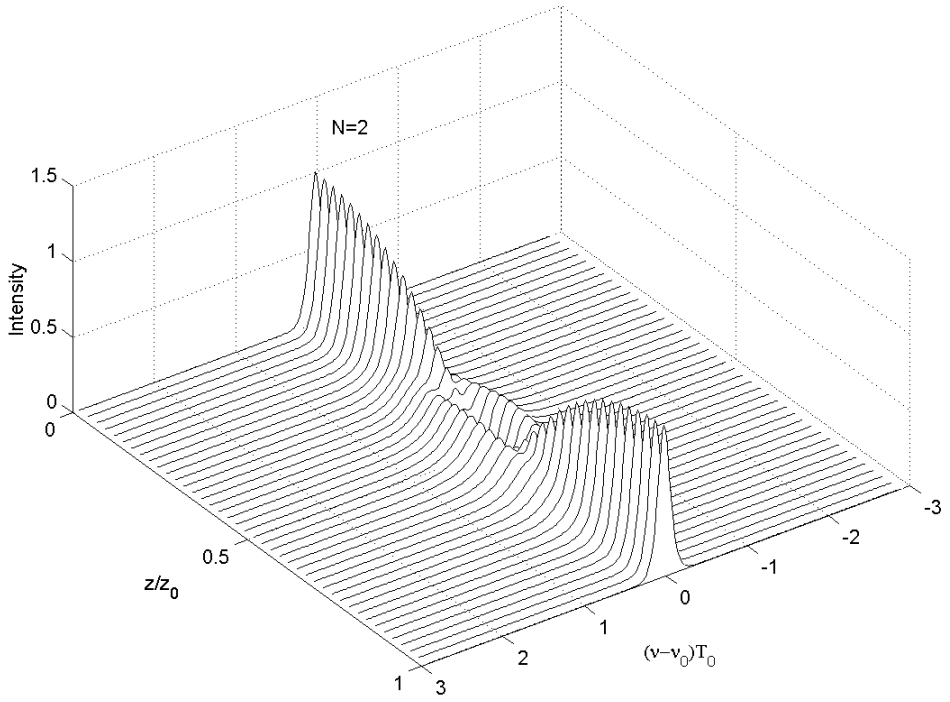

FIGURE 2.3b Spectral evolution of an N=2 soliton over one soliton period, z_0. The intensity is normalized to the input peak intensity.

2.4.3 Third-order soliton propagation (N=3)

Higher-order solitons show more complicated SPM-GVD interplay as the soliton order increases. Figure 2.4a and 2.4b show temporal and spectral evolution of N=3 soliton over one soliton period. The evolution is symmetric about $z_0/2$ and is repeated every z_0. At the initial stage of evolution, the pulse contracts with increasing intensity. It then splits into a two-peaked pulse near $z_0/2$. After $z = z_0/2$, pulse undergoes the reverse process. It merges again and recovers its initial shape.

Figure 2.5 shows the temporal shape, phase, chirp, and spectrum during N =3 evolution over one soliton period. In the initial stage of evolution (up to $z/z_0 = 0.25$), pulse compression is a dominant property. SPM generates positive chirp. Therefore the pulse contracts like a positively pre-chirped pulse in anomalous GVD region. Since the positive chirp is linear near over the pulse center, only this part of the pulse can contract. The rest of the pulse has negative chirp, so this portion becomes disperses and forms side lobes like a pulse shape at $z/z_0 = 0.25$ in Figure 2.5. The pulse intensity has its maximum at around $z/z_0 = 0.25$. The pulse spectrum of the initial stage shows the typical SPM-induced spectral broadening, clearly seen at $z/z_0 = 0.25$. Between 0.20 z_0 and 0.25 z_0, the energies at the offset frequencies pass through the pulse center. In Figure 2.5, the peak phase at $z/z_0 = 0.20$ has reached π radians and thereafter flips to $-\pi$, as shown in the phase plot at $z/z_0 = 0.25$. As a result, negative chirp appears across over the pulse center, as shown in the corresponding $\delta\omega$ plots. The pulse now begins to re-broaden as result of having negative chirp within the anomalous GVD region. Then the pulse begins to split apart at $z/z_0 = 0.35$, at which there are two regions of positive chirp on either side of a

region of negative chirp, as shown in the δω plot. With positive dispersion (D>0), the positively-chirped region of the pulse will be compressed, while the negatively-chirped region of the pulse will be broadened. This leads to a splitting of the pulse in time domain, as shown in the shape plot at z/z_0 = 0.40. After $0.5z_0$ the pulse evolution is exactly the reverse process. Chirp is completely anti-symmetric about $0.5z_0$. Since GVD is a linear process, the pulse shape can be recovered.

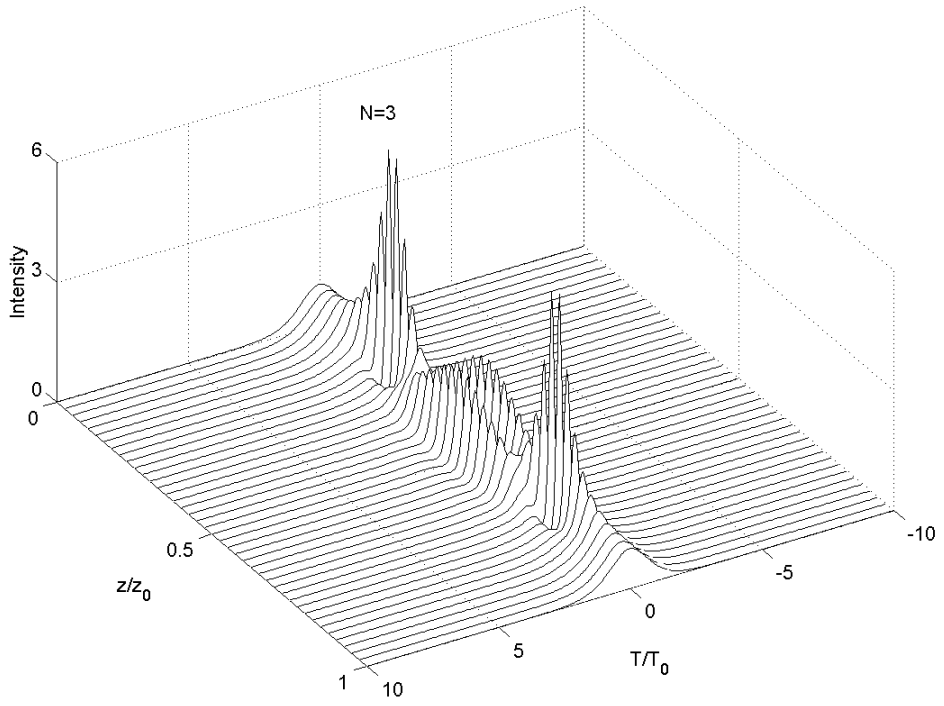

FIGURE 2.4a Temporal evolution of an N=3 soliton over one soliton period, z_0. The intensity is normalized to the input peak intensity.

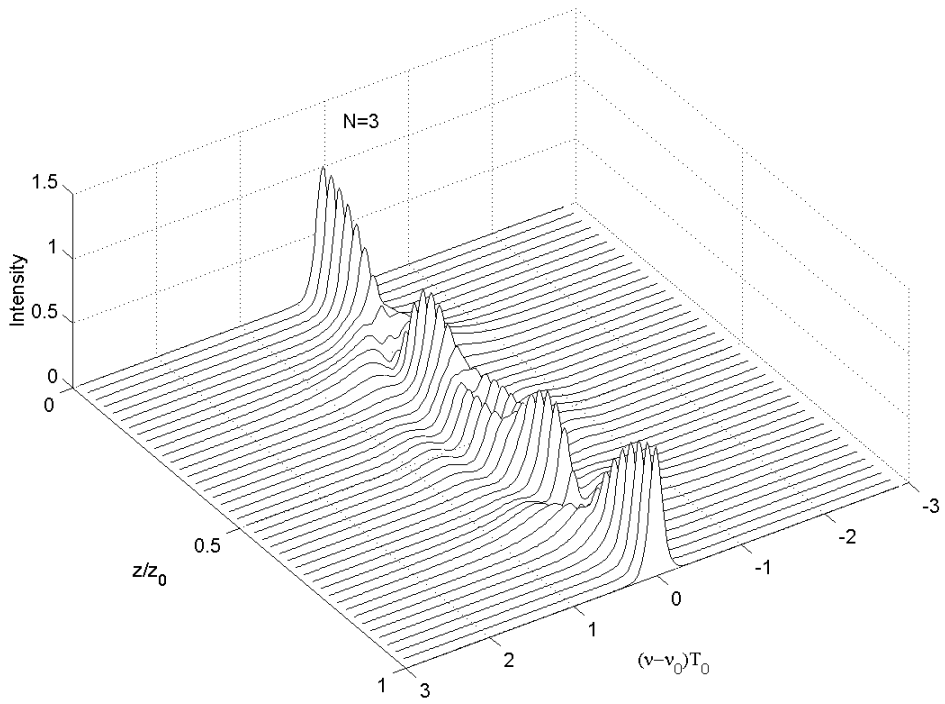

FIGURE 2.4b Spectral evolution of an N=3 soliton over one soliton period, z_0. The intensity is normalized to the input peak intensity.

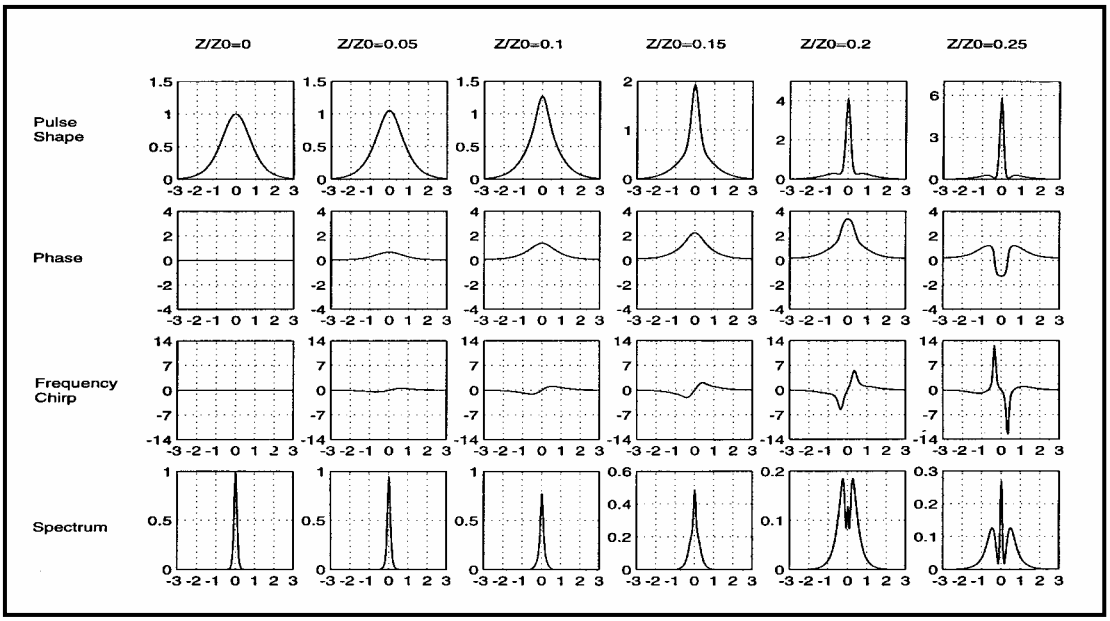

FIGURE 2.5 (with the following three pages) Soliton temporal envelope, nonlinear phase shift, frequency chirp, and pulse spectrum of an N=3 soliton over one soliton period, z_0.

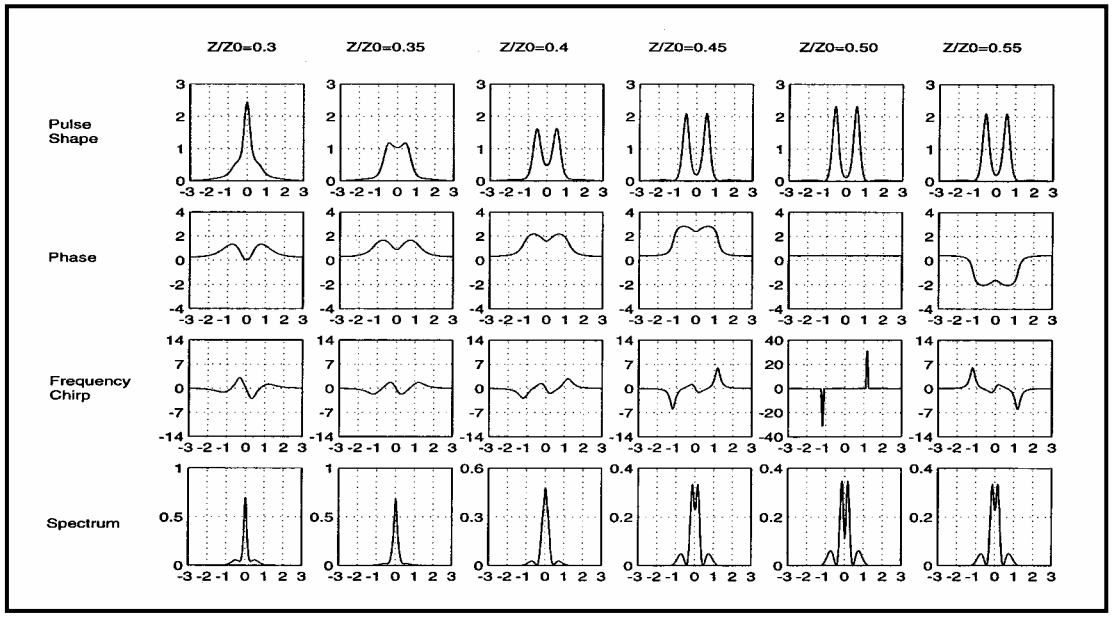

FIGURE 2.5 (continued)

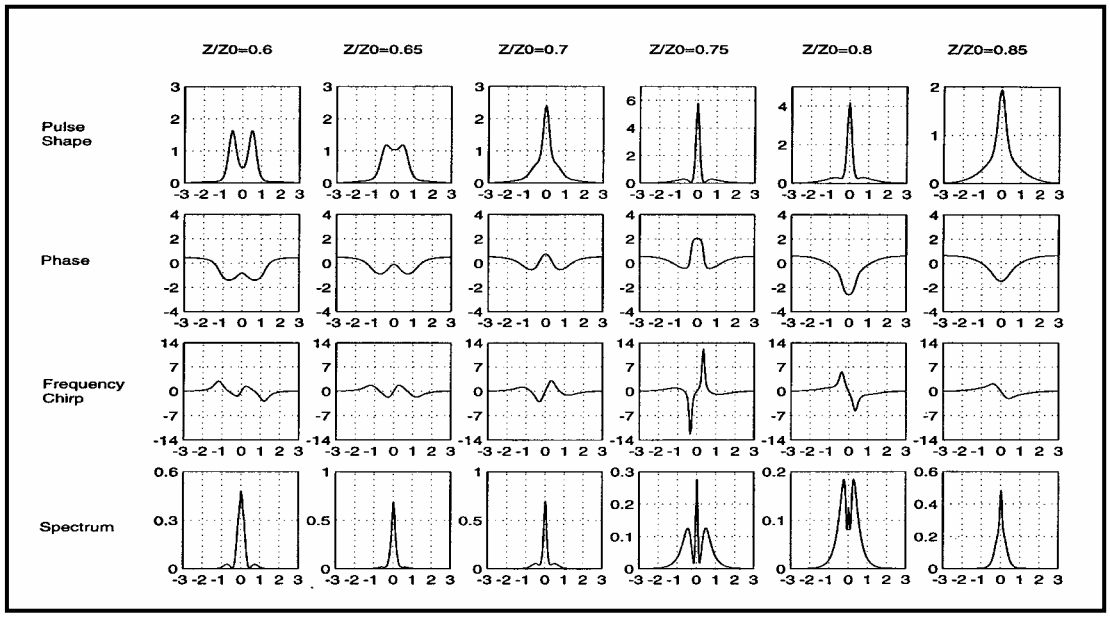

FIGURE 2.5 (continued)

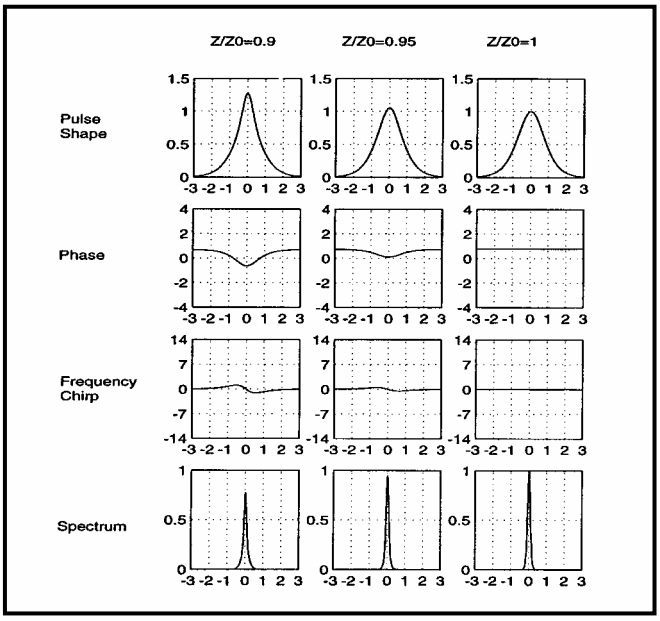

FIGURE 2.5 (continued)

CHAPTER 3

HIGHER-ORDER SOLTON DECAY USING LOCALIZED PERTURBATIONS

3.1 Introduction

In this chapter, we study the decay of higher order solitons in optical fibers. The decay of higher order solitons initiated by localized channel perturbations in the fiber will be proposed to obtain tunable wavelength separation. The perturbation is applied using a step change in dispersion, a loss element, or a bandpass filter. All result in the conversion of the soliton into two sub-pulses at wavelengths that are up and down-shifted from that of the input pulse. The wavelengths can be varied by adjusting the magnitude of the perturbation. Pulse parameter requirements for achieving useful wavelength shifts while avoiding unwanted nonlinear effects are presented. In principle, the converted pulses can be amplified to form separate higher order solitons, and the process repeated to produce multiple wavelengths of variable spacing; care is required, however, to assure that detrimental effects associated with amplification, such as amplified spontaneous emission (ASE), are avoided [20].

3.2 Physical Perspective

Our studies center on the response of solitons of order N=2 or N=3 to the aforementioned three perturbations. As diagramed in Figure 3.1, during the unperturbed evolution of these solitons with distance, wavelength spectra broaden and separate into two peaks (for N=2) or three peaks (for N=3), where in the latter case, the original center wavelength is retained. The maximum spectral separation, $\Delta\lambda_{max}$, occurs at locations corresponding to 0.5 z_0 for N=2 and 0.25 z_0 for N=3. As is well-known, further propagation results in the spectra re-compressing to form the original input. The process repeats, completing the cycle each soliton period distance, z_0. While spectra are separated, the soliton in time domain can be thought of as two or three overlapping pulses that are associated with the separated spectral components.

Figure 3.2 and Figure 3.3 show our soliton decay methods for N=2 and N=3 solitons respectively. Our method involves placing the perturbations at the $\Delta\lambda_{max}$ locations, where the maximum spectral separation occurs, corresponding to 0.5 z_0 for N=2 and 0.25 z_0 for N=3 (see Figure 3.1). By doing so, the nonlinear response of the fiber beyond the perturbation is effectively reduced, thus preventing the complete return of the spectrum to its original form. The composite pulses, retaining their individual spectra, separate in time owing to their different group velocities. The reduced nonlinear response beyond the perturbation then participates in the continued evolution of the separated pulses in the following ways: 1) the sub-pulses may evolve into fundamental solitons or nearly so — i.e., into pulses that exhibit little change over several dispersion distances; 2) the spectrum partially re-compresses, leading to a wavelength spacing between sub-

pulses that is less than the value just before the perturbation. Consequently, by varying the magnitude of the perturbation (equivalent to varying the nonlinear strength in the channel beyond the perturbation), the wavelength spacing between the sub-pulses, $\Delta\lambda$, can be varied.

Maximum wavelength spacings obtainable for N=2 and N=3, as a functions of FWHM input pulse width, are plotted in Figure 3.4 for a 1.55 μm center wavelength. As an example, if a 10 ps pulse is used, a maximum spacing for N=2 of $\Delta\lambda_{max}$=0.8nm (100 GHz) can be obtained by using a large perturbation at the 0.5 z_0 position. The wavelength spacing can be reduced from this value by weakening the perturbation. If an N=2 soliton is used, only the shifted wavelengths remain in the signal. For an N=3 soliton, sub-pulses are generated that can have a larger wavelength spacing than those in an N=2 pulse, and a relatively weak pulse at the original carrier wavelength remains.

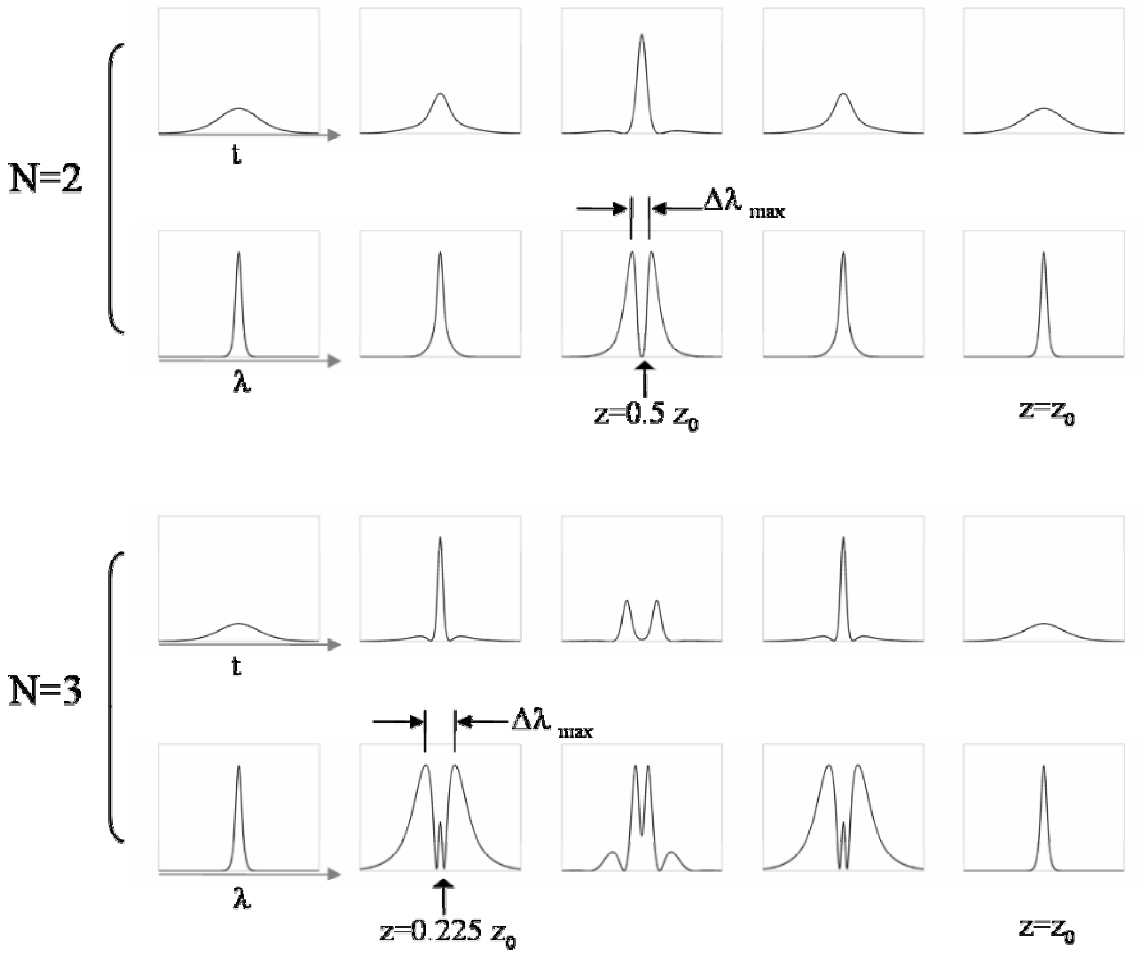

FIGURE 3.1 Temporal and spectral evolution of unperturbed N=2 and N=3 solitons at selected positions in the fiber channel. Perturbation locations used in this work are indicated.

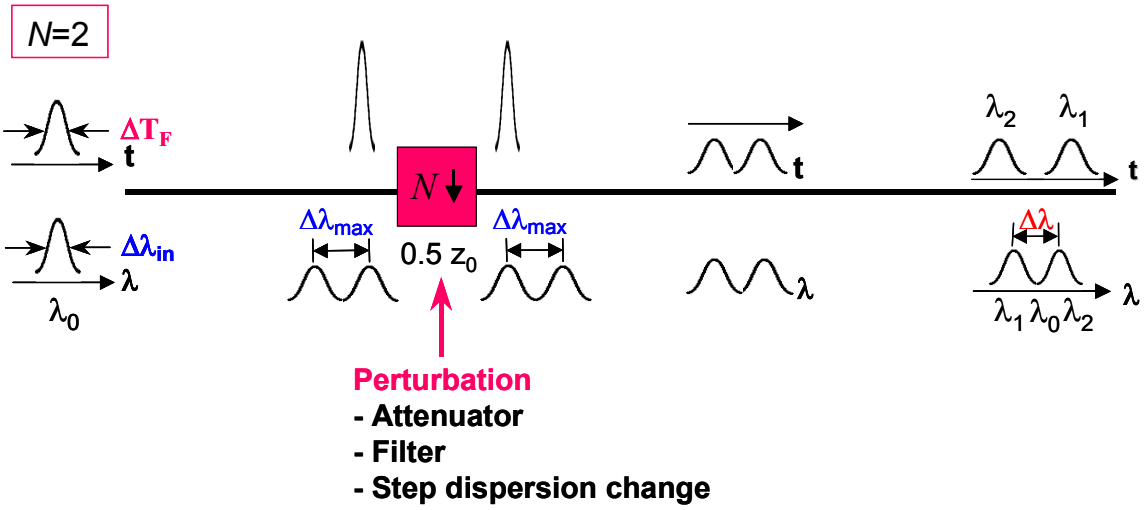

FIGURE 3.2 Temporal separation of the N=2 soliton spectral components as a result of a perturbation applied at the half soliton period distance. The perturbation reduces the value of the soliton number, N, and so only partial spectral re-compression occurs. Fundamental solitons at the separated wavelengths may evolve if a dispersion step perturbation is used.

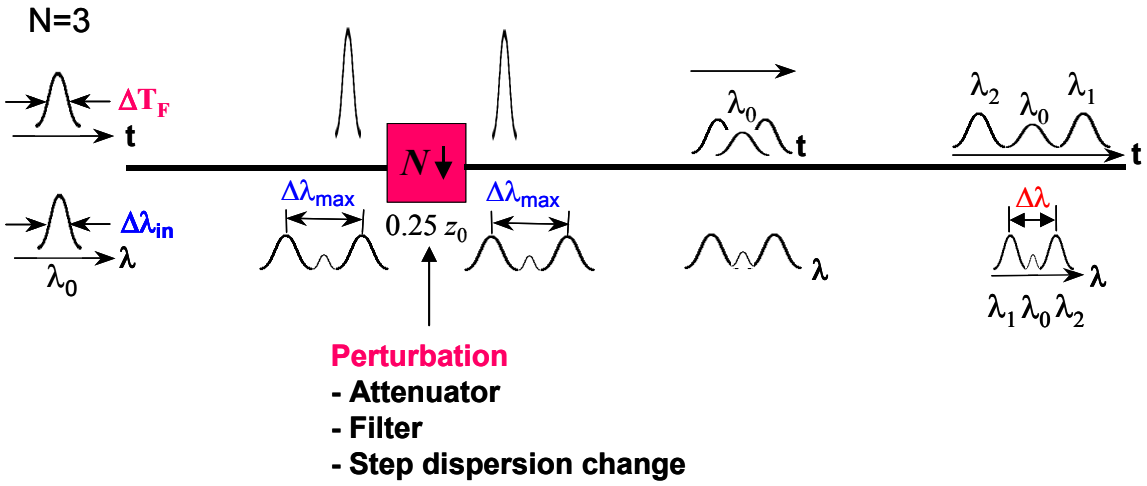

FIGURE 3.3 Temporal separation of the N=3 soliton spectral components as a result of a perturbation applied at the half soliton period distance. The perturbation reduces the value of the soliton number, N, and so only partial spectral re-compression occurs. Fundamental solitons at the separated wavelengths may evolve if a dispersion step perturbation is used.

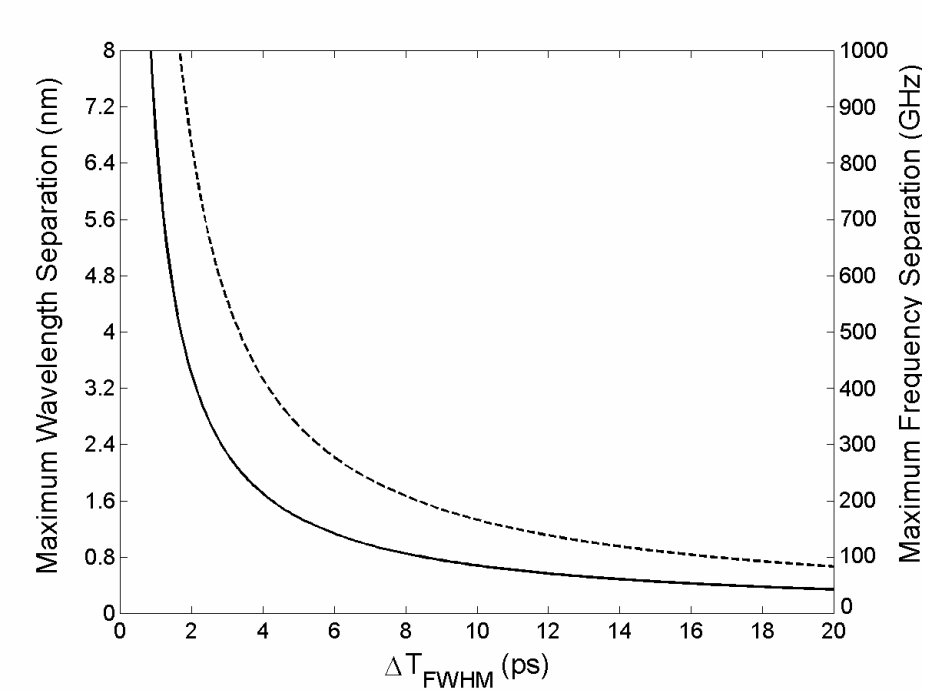

FIGURE 3.4 Maximum obtainable wavelength separations $\Delta\lambda_{max}$ as functions of input pulse width for N=2 (solid curve) and N=3 (dashed curve) solitons. The corresponding frequency separations at 1.55 μm wavelength are indicated on the right vertical axis.

3.3 Numerical Results

To investigate the soliton decay, we solved the equation (2.2.6) given by:

$$\frac{\partial U}{\partial z} - \frac{i}{2}\frac{\partial^2 U}{\partial \tau^2} - \delta\frac{\partial^3 U}{\partial \tau^3} = iN^2\left[|U|^2 U + is\frac{\partial}{\partial \tau}(|U|^2 U) - \tau_R U\frac{\partial}{\partial \tau}(|U|^2)\right].$$

As described in Section 2.2, U is the normalized complex envelope of the pulse, ξ is the normalized distance, and τ is the normalized local time. The cubic dispersion, self-steepening, and Raman response parameters are respectively given by $\delta=\beta_3/(6|\beta_2|T_0)$, $s=1/(T_0\omega_0)$, and $\tau_R=T_R/T_0$. The initial envelope of the soliton at $\xi = 0$ is given by $U(0,\tau)=\text{sech}(\tau)$.

The soliton order, N, in the above equation provides a measure of the strength of the nonlinear response, compared to the fiber dispersion. Applying the perturbation effectively reduces the value of N for all positions at and beyond the point of application. From (2.2.7), it is seen for example that N is decreased by increasing D or by decreasing P_0, the latter being accomplished in our case by a loss element or a bandpass filter. With the perturbation applied, the separated pulses may evolve into fundamental solitons, provided energy is not removed from the pulse pair. A step increase in dispersion will satisfy this requirement, whereas a loss element or filter will not.

The effects of δ, s, and τ_R are described in detail later. To minimize their contributions, pulses must be sufficiently broad to enable modest peak powers and longer rise and fall times, while satisfying the higher order soliton condition. Consequently, we are constrained to input pulses of widths $T_0>1$ps such that $T_0\omega_0>>1$ and $T_R/T_0<<1$, at

which δ, s, and τ_R can be negligible [19]. Under this constraint, but nevertheless including all higher order terms, the NLSE was solved using the split-step Fourier method, in which a reduction in pulse amplitude or bandwidth, or an increase in fiber dispersion was incorporated at the maximum bandwidth positions.

Figure 3.5 shows the separation of ΔT_f =1 ps sub-pulses originating in an N=2 soliton after a step increase in dispersion at the $z_0/2$ location. Using a transition to higher dispersion fiber effectively reduces the value of N, while maintaining the pulse energy, thus enabling the sub-pulses to evolve into fundamental solitons. In this example, the initial dispersion is 8 ps/nm-km (for z=0 to $0.5z_0$) and is step-increased to 16 ps/nm-km (for $z=0.5z_0$ to $2.5z_0$). As shown in Figure 3.5, the separation between the two pulses increases linearly with the distance, indicating group velocity differences arising from their having different center wavelengths. This is confirmed by the spectrum (Figure 3.5a inset). Increasing the run time, allowing further propagation over several dispersion lengths yielded no discernable change in pulse shape or width.

Sub-pulse formation from N =3 solitons using the same dispersion change as in Figure 3.5 are shown in Figure 3.6, except the position of the dispersion step is at $z=0.225\ z_0$. In this case, the original soliton decays into two sub-pulses at the shifted wavelengths, with a remnant of the original carrier wavelength surviving as a third weaker pulse. The spectral separation between pulses is greater than that in the N=2 case, and again, no discernable change in the wavelength-translated pulses was found after propagating through several dispersion lengths.

The plots in Figure 3.5 show results under lossless propagation. When including fiber loss of 0.2 dB/km, the effect is negligible for pulse widths on the order of 1 ps. With longer pulses, the dispersion length (proportional to the square of the pulse width) may be sufficiently long to affect the pulse energy during the evolution process. The effects are 1) a longer distance is needed to achieve $\Delta\lambda_{max}$ (for example $0.55z_0$ instead of $0.5\ z_0$ for a 10 ps N=2 input), and 2) the expected power reduction with distance of the output fundamental solitons occurs, along with their eventual dissipation.

As an alternative to a dispersion step, use of an attenuator or a filter reduces the nonlinear response beyond the perturbation by removing energy from the pulse. Figure 3.7 and 3.8 show the separation of ΔT_f =1 ps sub-pulses originating in an N=2 soliton after 3dB attenuation and bandbass filtering at the $z_0/2$ location respectively. The transformed pulses appear similar to those shown in Figure 3.5, but decay asymptotically to eventually dissipate. Nevertheless, they were found to exhibit almost chirp-free fundamental soliton behavior over several dispersion lengths, even when distributed losses were included.

Wavelength spacings between sub-pulses as functions of the dispersion difference, attenuation, and filter bandwidth ($\Delta\lambda_f$) of the channel perturbation are plotted in Figure 3.9 for N=2 and N=3. In Figure 3.9, the wavelength spacing and the filter width are normalized with respect to the input spectral width $\Delta\lambda_{in}$ (in turn inversely proportional to the input pulse width). The bandpass filter has a Gaussian shape, and is centered at the input pulse carrier frequency. When a dispersion step or an attenuator is used, the wavelength separation increases toward the maximum allowable value (as can be

determined from Figure 3.4) as the perturbation magnitude increases. For example, wavelength spacings from 0 to 10 nm are predicted for a 1ps input pulse by changing dispersion between 10-80% or by attenuating the signal between 1 and 5 dB. On the other hand, when using a filter, the perturbation magnitude increases with decreasing filter width. The curves in Figure 3.9c are seen to reach local maxima, and then fall off as the filter width becomes narrower. This would be expected, since the filter itself would eventually block transmission of the more widely-spaced spectral components.

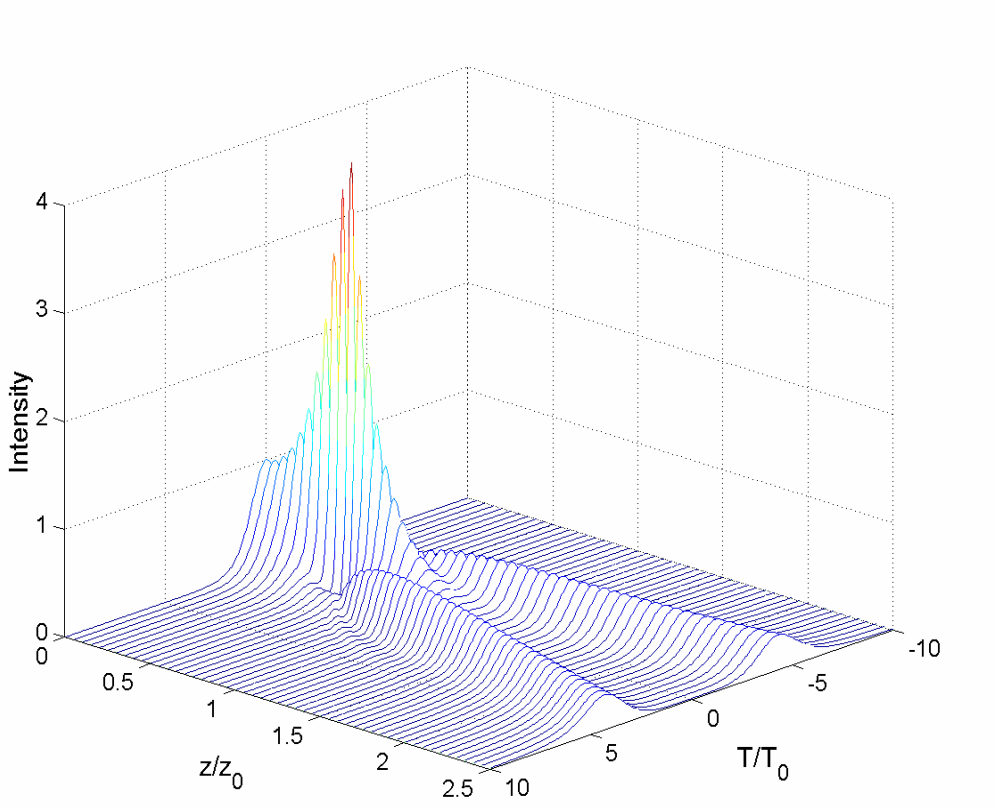

(a)

FIGURE 3.5 Numerical results, showing the decay of an N=2 soliton, initiated by a step-increasing the dispersion from 8 ps/nm-km to 16 ps/nm-km at the position, z/z_0=0.5. Temporal (a) and spectral (b) evolution on next page show the formation of nearly fundamental solitons at two wavelengths.

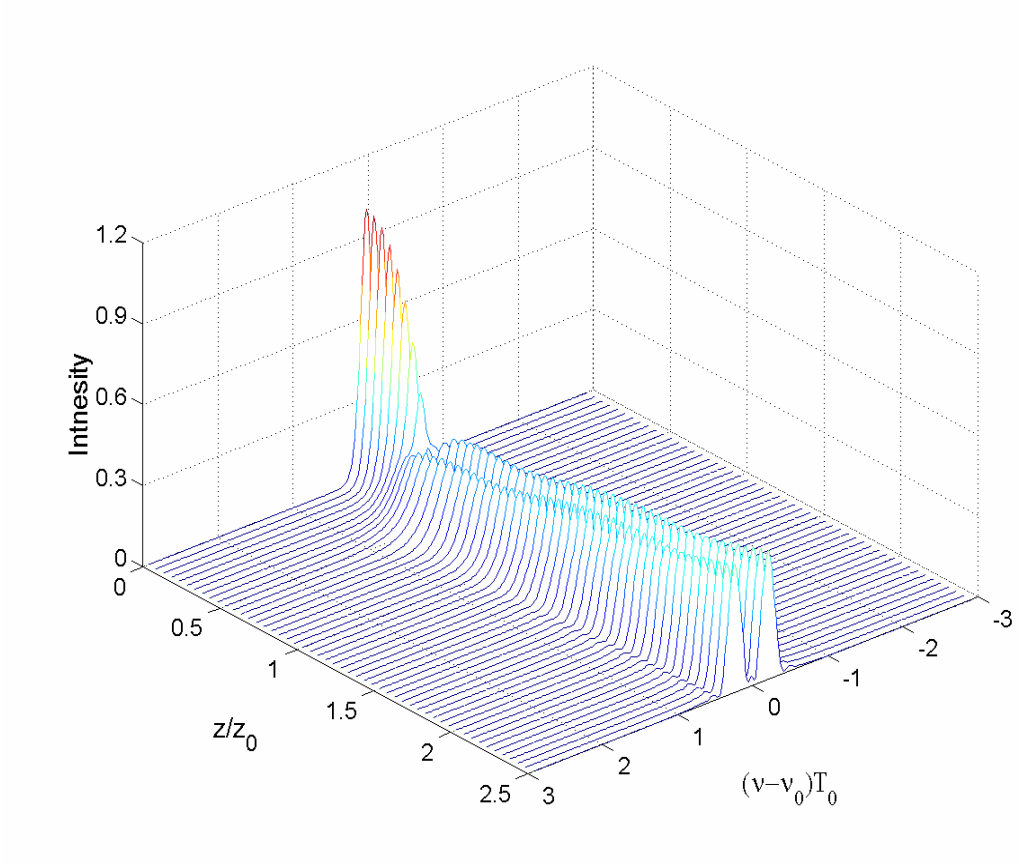

(b)

FIGURE 3.5 (continued)

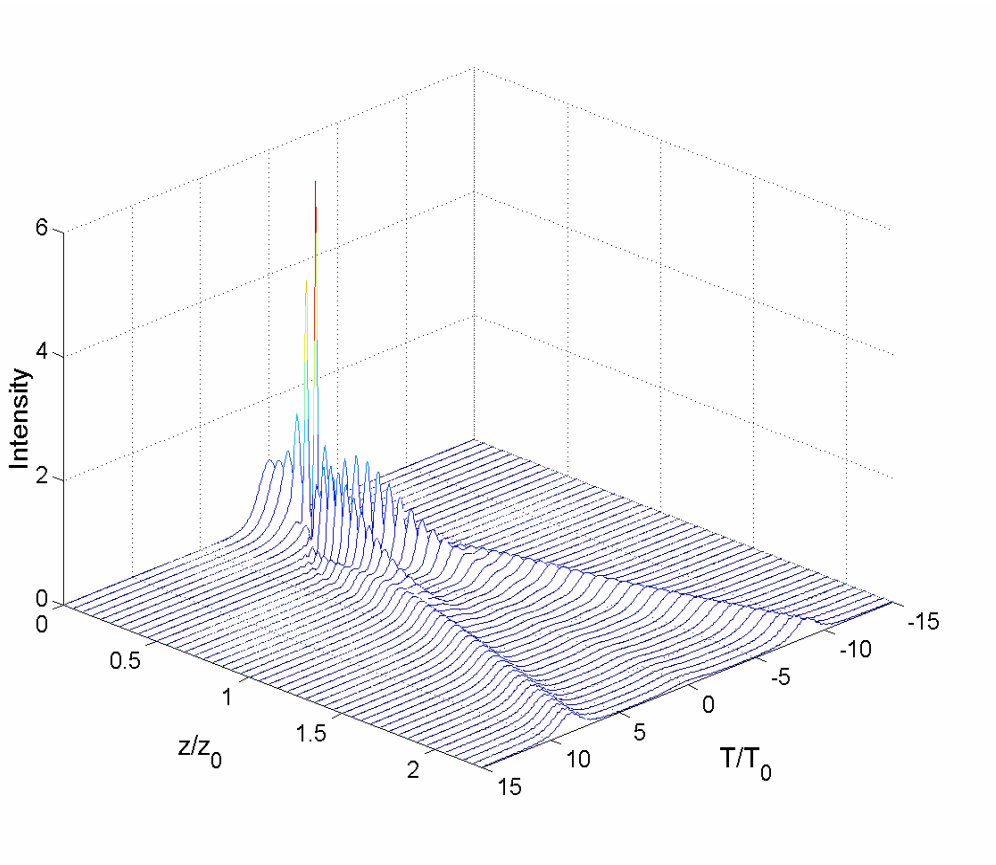

(a)

FIGURE 3.6 Numerical results, showing the decay of an N=3 soliton, initiated by a step-increasing the dispersion from 8 ps/nm-km to 16 ps/nm-km at the position, z/z_0=0.25. Temporal (a) and spectral (b) evolution on next page show the formation of nearly fundamental solitons at three wavelengths.

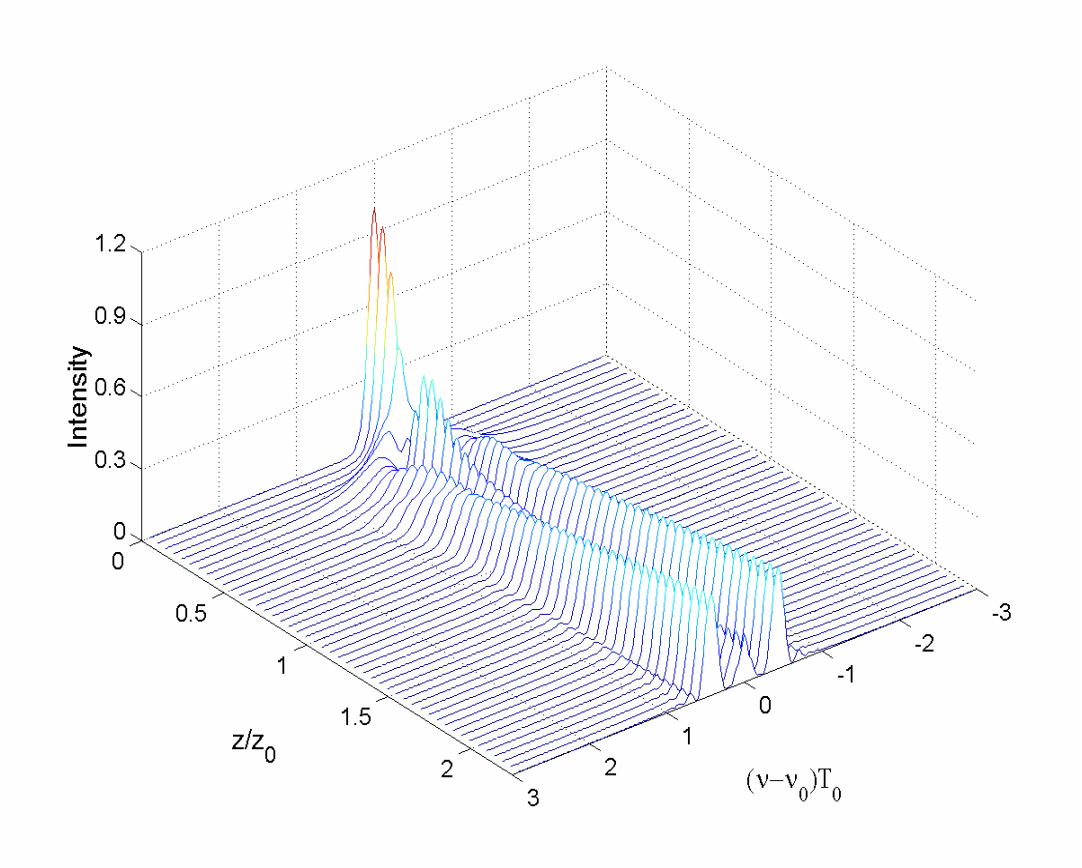

(b)

FIGURE 3.6 (continued)

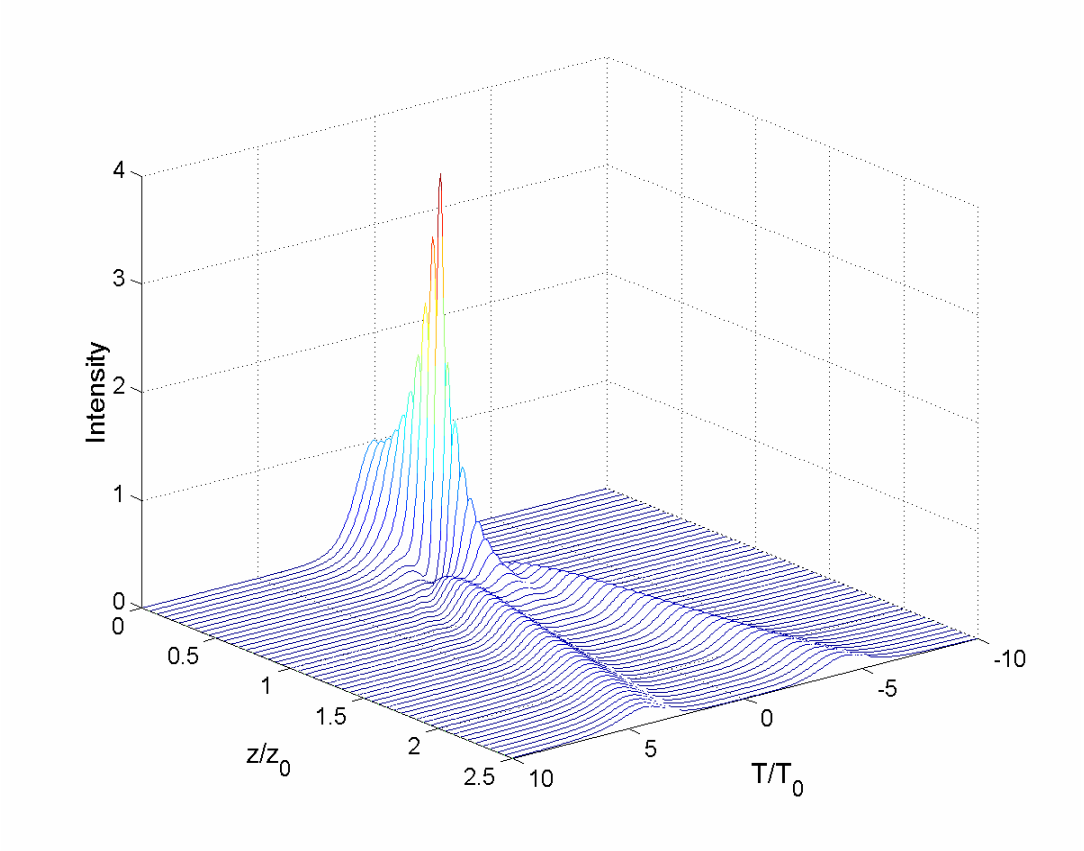

(a)

FIGURE 3.7 Numerical results, showing the decay of an N=2 soliton, initiated by attenuation (3dB) at the position, z/z_0=0.5. Temporal (a) and spectral (b) evolution on next page show the formation of subpulses at two wavelengths.

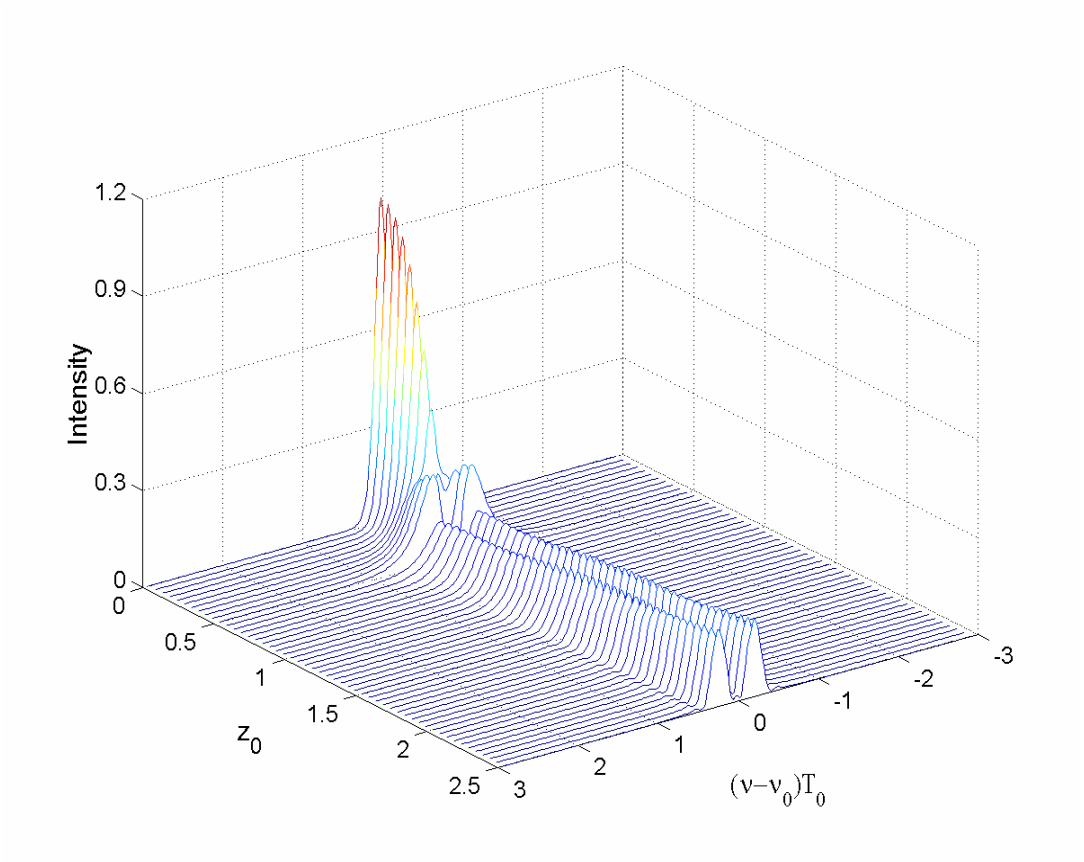

(b)

FIGURE 3.7 (continued)

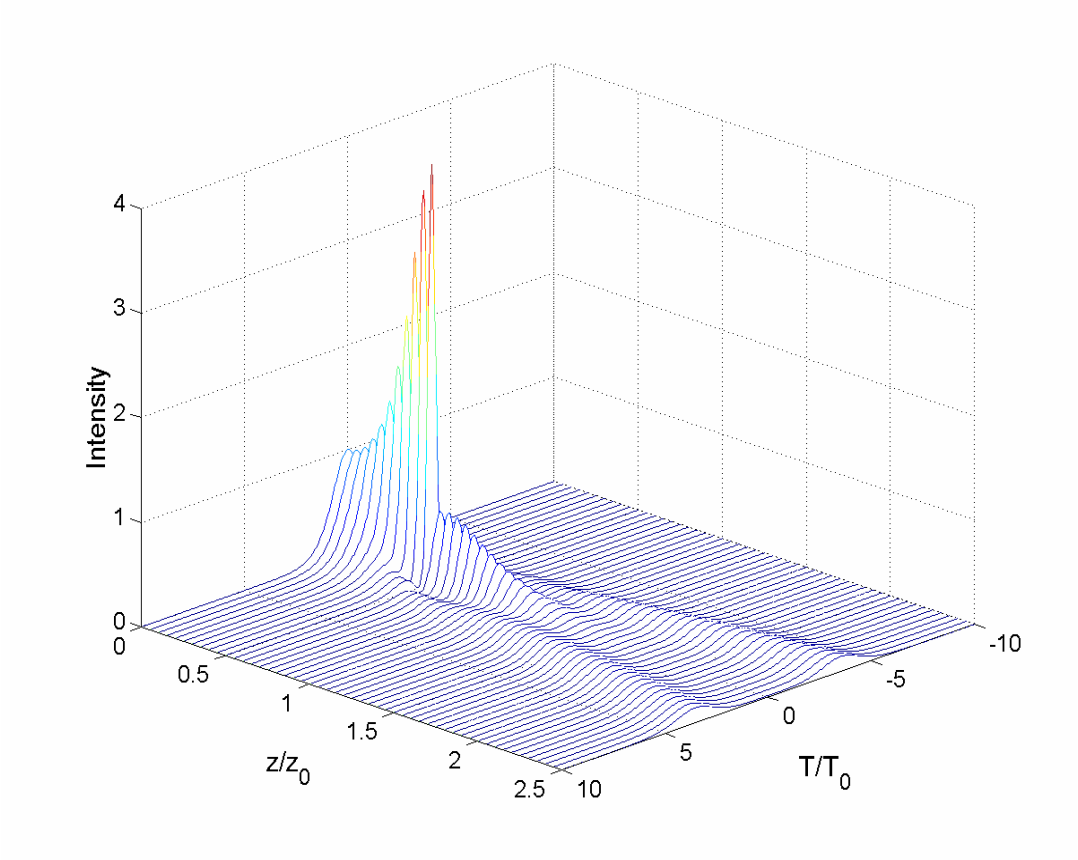

(a)

FIGURE 3.8 Numerical results, showing the decay of an N=2 soliton, initiated by bandpass filtering ($\Delta\lambda_f/\Delta\lambda_{in}$ = 2.72) at the position, z/z_0=0.5. Temporal (a) and spectral (b) evolution on next page show the formation of subpulses at two wavelengths.

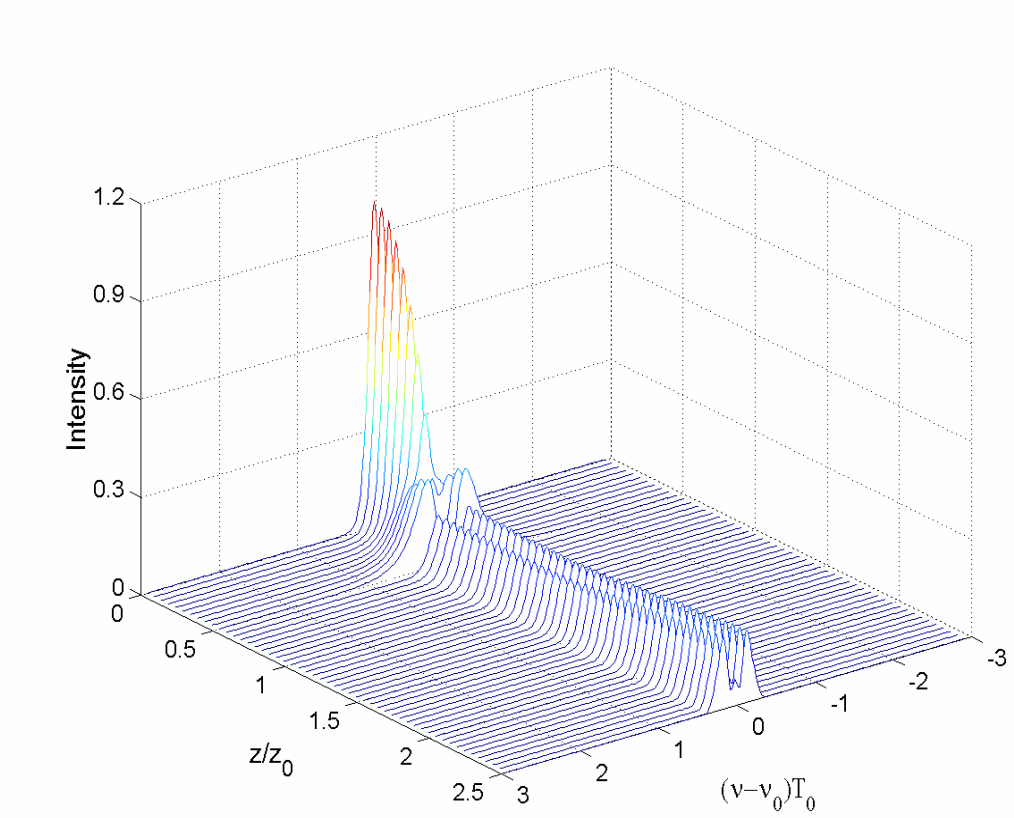

(b)

FIGURE 3.8 (continued)

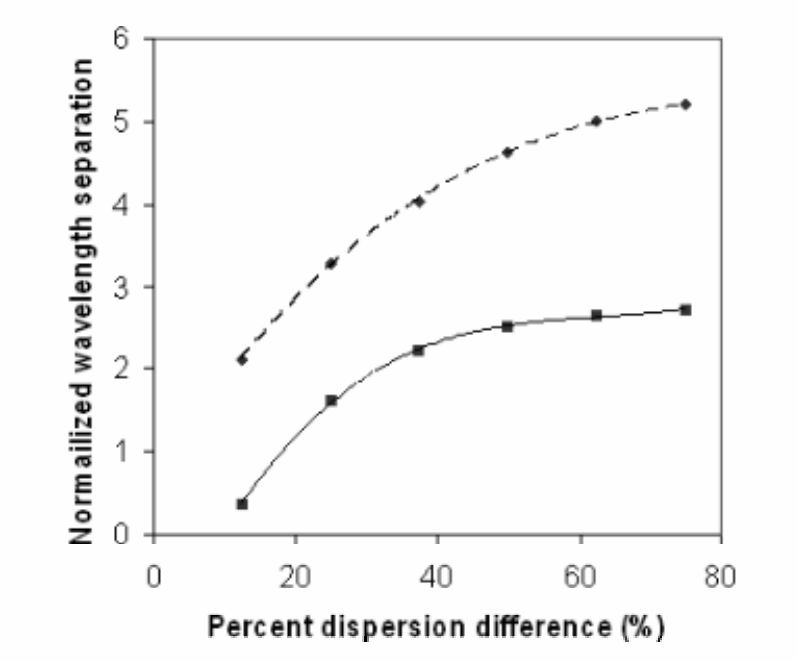

(a)

FIGURE 3.9 Wavelength separations obtained as functions of dispersion difference (a), attenuation (b), and filter bandwidth (c) for N=2 solitons (solid curves) and N=3 solitons (dashed curves). Wavelength separation and filter bandwidth are normalized with respect to the input FWHM spectral width.

.

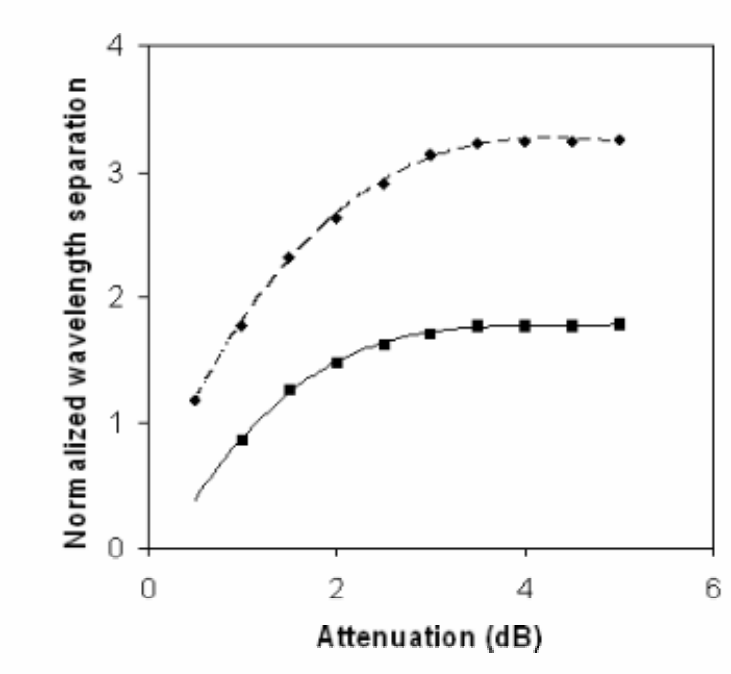

(b)

FIGURE 3.9 Wavelength separations obtained as functions of dispersion difference (a), attenuation (b), and filter bandwidth (c) for N=2 solitons (solid curves) and N=3 solitons (dashed curves). Wavelength separation and filter bandwidth are normalized with respect to the input FWHM spectral width.

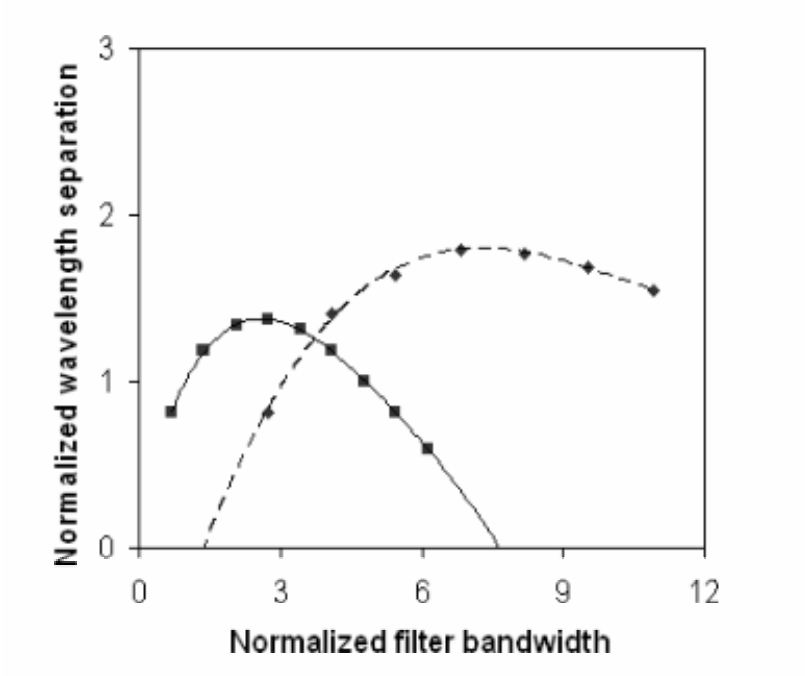

(c)

FIGURE 3.9 Wavelength separations obtained as functions of dispersion difference (a), attenuation (b), and filter bandwidth (c) for N=2 solitons (solid curves) and N=3 solitons (dashed curves). Wavelength separation and filter bandwidth are normalized with respect to the input FWHM spectral width.

3.4 Higher-Order Effects

When pulse widths are reduced to values on the order of a few picoseconds or less, the higher order terms in Equation (2.2.6) involving δ, s, and τ_R can become appreciable and may lead to degradation of the signal after the perturbation. These were studied for the N =2 soliton case. The most important of the three, appearing with input pulse widths of ΔT_f =1 ps and shorter, is Raman scattering; this has the effect of shifting energy from the shorter wavelength into the longer wavelength pulse, leading to an amplitude imbalance between the two pulses, in a manner observed in non-perturbed N=2 solitons [11]. In addition, both pulses experience a self frequency shift to longer wavelengths. These effects, shown in Figure 3.7, become more pronounced as input pulse widths become shorter, and ultimately prevent sub-pulse evolution into fundamental solitons, as expected [10]. The cubic dispersion term was found to introduce a slight asymmetry in the overall signal envelope which tends to counter-act the imbalance arising from the Raman effect. This effect, observed previously in N=2 solitons [21], imparts a slight correction to the Raman imbalance, but again is negligible for pulse widths of 1 ps and longer. The self steepening term was found to have a negligible effect for pulse widths above ΔT_f =0.1 ps. All three processes are thus avoided for N=2 solitons with input pulse widths of ΔT_f >1 ps.

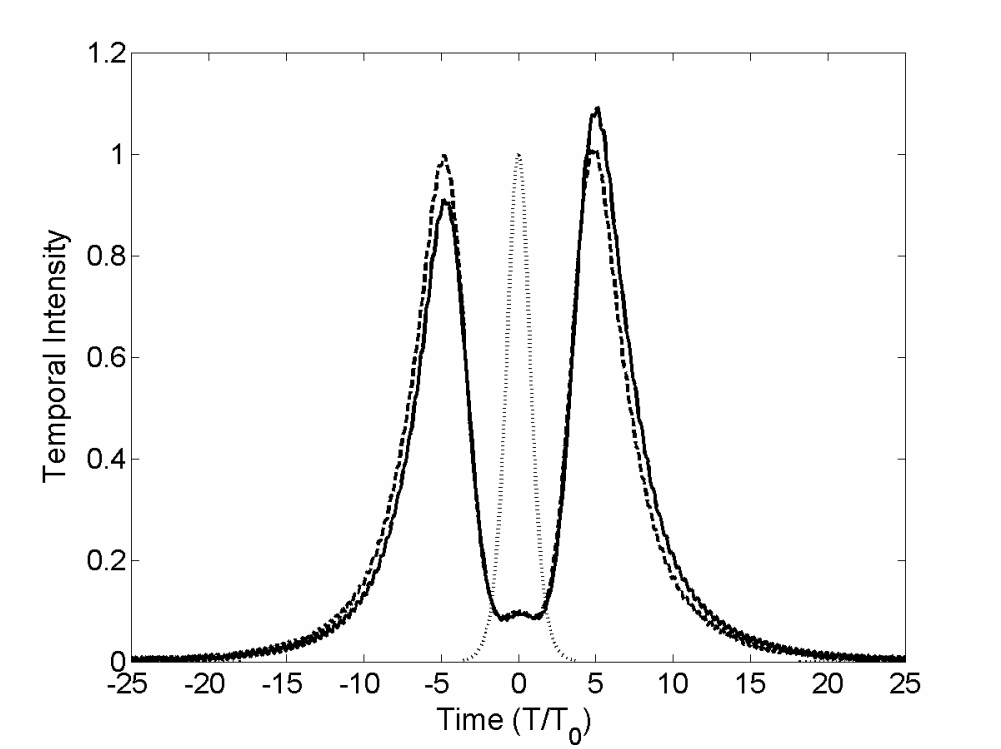

FIGURE 3.10a Normalized temporal plots showing the effects of cubic dispersion and Raman scattering on the separated pulses after stepping up the dispersion. The dotted traces are those of the input pulse. Solid traces correspond to a 10 ps input pulse width. Dashed traces correspond to a 1 ps input width

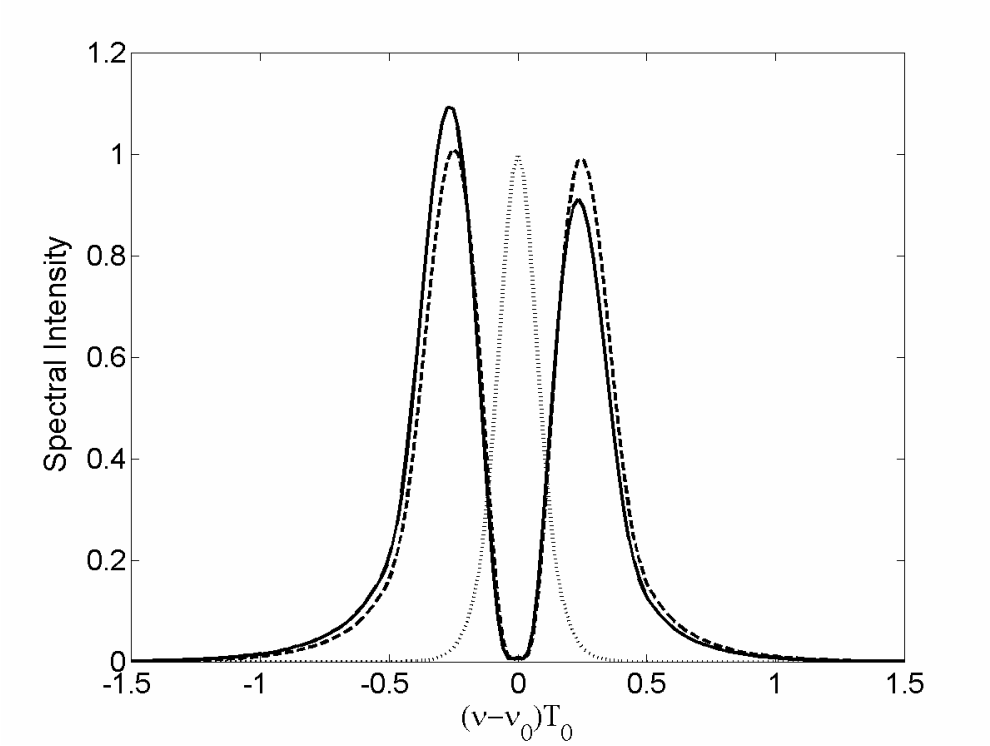

FIGURE 3.10b Normalized spectral plots showing the effects of cubic dispersion and Raman scattering on the separated pulses after stepping up the dispersion. The dotted traces are those of the input pulse. Solid traces correspond to a 10 ps input pulse width. Dashed traces correspond to a 1 ps input width

CHAPTER 4

EXPERIMENTS ON WAVELENGTH CONVERSION USING *N*=2 SOLITON DECAY

4.1 Introduction

In the previous chapter, the decay of higher order solitons in optical fiber, initiated by a step change in dispersion or by a localized loss element or filter, is explored numerically as a means of generating pairs of pulses having wavelengths that are up and down-shifted from the input wavelength. The wavelengths are tunable by varying the magnitude of the perturbation. In this chapter, we propose a tunable wavelength conversion method using the controlled decay of N=2 solitons. Tunable wavelength conversion using N=2 soliton decay initiated by a step change in dispersion will be demonstrated experimentally. Obtainable wavelength separations as a function of the dispersion difference will be measured for a 1 ps soliton pulse. Stability of the wavelength conversion process will be investigated.

4.2 Experiments Using a Step Change in Dispersion

We have shown that the higher-order soliton decay initiated by localized channel perturbations could generate pairs of pulses having wavelengths that are up and down-shifted from the input wavelength. Using the higher-order soliton decay, it is possible to generate two copies of an optical data stream, in which the copies are at wavelengths that differ from that of the original data. This proposed wavelength conversion method is very simple and in principle error-free. The process can in principle be repeated to produce multiple wavelength replicas of an input data stream, and may thus be of possible use in multi-casting applications in fiber communication systems. In this section, we experimentally demonstrate a tunable wavelength conversion using N=2 soliton decay initiated by a step change in dispersion.

Figure 4.1 shows the experimental setup for N=2 soliton decay. A figure-8 laser (F8L) is used to produce a soliton pulse. The 1-ps FWHM output from a figure-8 laser (F8L) was amplified by an erbium-doped fiber amplifier (EDFA) and then launched at location A such that its pulse width and intensity satisfied the N=2 soliton condition within the initial low-dispersion fiber (LDF) section. The center wavelength was 1550 nm and the peak power was 36 W. The amplifier introduced low-level spectral features on the pulse that are associated with amplified spontaneous emission (ASE). Simulations showed these features to have negligible effect on the pulse evolution.

For a transition to higher dispersion fiber at one-half the soliton period for N=2, we use a half soliton period of a low dispersion fiber (LDF) and two soliton periods of a corning SMF-28 fiber. The dispersion parameter of the LDF at 1550 nm is 4.3 ps/km/nm,

and its mode field diameter (MFD) is 8.4 μm. For the SMF-28, the dispersion parameter at 1550 nm is 17 ps/km/nm, and its MFD is 10.4 μm. Using a transition to a higher dispersion fiber effectively reduces the value of N while maintaining the pulse energy. The result is the formation of two fundamental solitons at the separate wavelengths.

Autocorrelation traces and spectral measurements at each stage (from locations A to C) are shown in Figure 4.2, along with results of the numerical simulations for a 1 ps (FWHM) N=2 soliton with ΔD = 75%. Measurements at position B confirmed the expected N=2 soliton temporal compression and spectral separation at the $z_0/2$ location. The increase in dispersion to 17 ps/nm-km at B lowers the nonlinear response in the B-C segment, allowing the two sub-pulses to temporally separate and dispersively broaden, as confirmed by the autocorrelation measurement at position C. These results were found to be in excellent agreement with numerical simulations, shown as the dashed traces in Figure 4.2. The spectrum at point B ($z=0.5z_0$) shows the maximum wavelength separation. Measured and simulated maximum wavelength separations are 6.2 nm and 6.9 nm respectively. About a 10 dB dip is observed between the two separated wavelength components. The measured autocorrelation trace at position C in Figure 4.2 shows 3 peaks, which confirms that two sub-pulses are formed at this position. Measured and simulated wavelength separations between two subpulses at the end of the SMF-28 are 6.1 nm and 6.7 nm respectively.

Wavelength separations at position C as a function of the dispersion difference are measured at three data points. They are plotted in Figure 4.3 for the N=2 soliton case. The solid curve indicates a simulation result. The wavelength separation is normalized

with respect to the input spectral width (in turn inversely proportional to the input pulse width). The experimental results are in a good agreement with the simulation results.

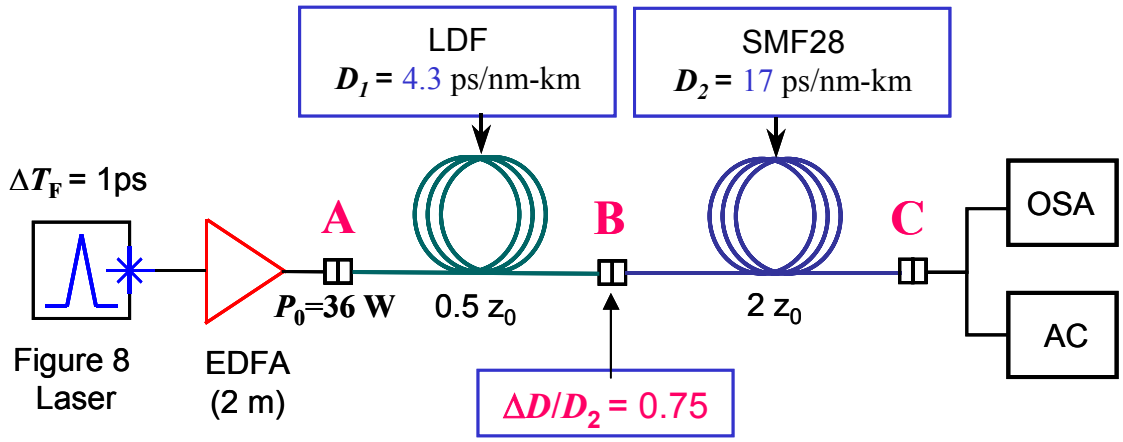

FIGURE 4.1 Experimental setup for N=2 soliton decay using a step increase in dispersion; OSA: Optical Spectrum Analyzer and AC: Auto-Correlator.

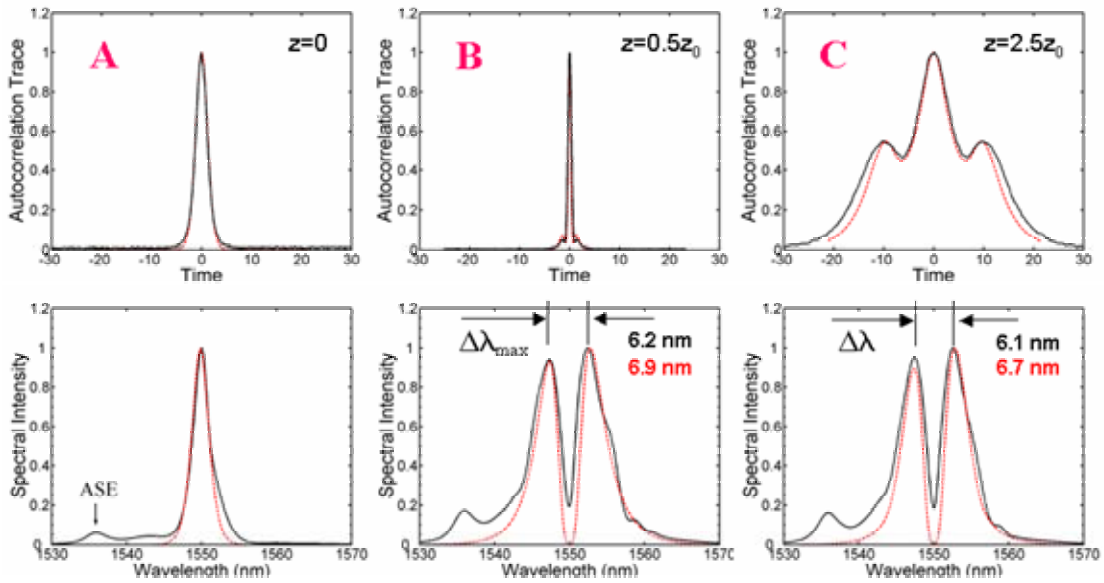

FIGURE 4.2 Measured (solid line) and simulated (dashed line) autocorrelation traces and spectra at the z/z_0= 0, 0.5, and 2.5 for a 1 ps (FWHM) N=2 soliton with ΔD = 75%.

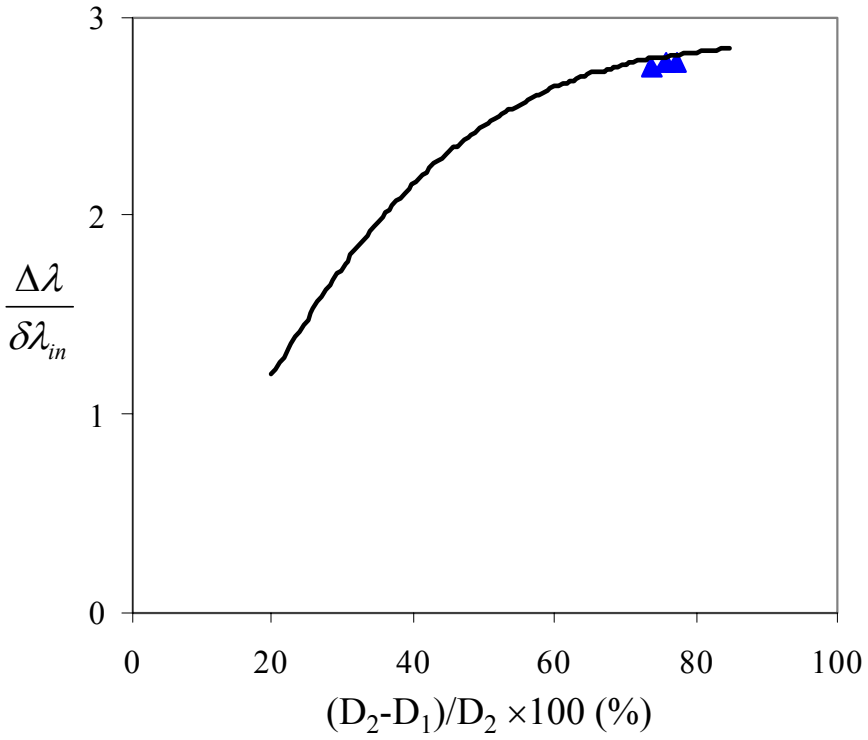

FIGURE 4.3 Measured wavelength separations as function of dispersion difference; solid line indicates a simulation result. The wavelength separation is normalized with respect to the input spectral width.

4.3 Stability of Wavelength Conversion

In this section, stability or robustness of the wavelength conversion process will be investigated. The main emphasis is on the sensitivity of wavelength separation to fluctuations in power and/or variations in the perturbation locations in the fiber channel.

For practical applications of the proposed wavelength conversion method, stability or robustness of the system is an important factor. Figure 4.4 shows the simulation and experimental studies on the sensitivity of wavelength separation to power fluctuations in the fiber channel. An input power decrease by a given percentage results in approximately twice that percentage decrease in spectral separation. Increasing the input power beyond the N=2 condition slightly increases the spectral separation, which eventually saturates to a maximum. Therefore, the sensitivity of the system to power fluctuations in the fiber channel can be decreased significantly by operating the wavelength conversion in the saturation region. Discrepancy between measured and simulated wavelength separation increases as the input power increases. This may result from using larger Raman response parameters in the simulation because the effect of stimulated Raman scattering on wavelength separation tends to increase wavelength separation when the input power is high.

The perturbation location in practical implementation may differ from the theoretical location, where the maximum wavelength separation occurs (seen in Figure 4.1). The simulation studies on the sensitivity of wavelength separation to variations in the perturbation locations in the fiber channel have been performed. Figure 4.5 shows the output spectra obtained when changing the perturbation location from the maximum

wavelength separation location (0.50 z_0) to 0.45 and 0.55 z_0. The resulting wavelength separations are seen to change slightly (within ±10 percent). This result shows that the system is robust to variations in perturbation location in the fiber channel.

The effect of using non-soliton pulses, whose pulse shapes and spectra may differ from those of the exact soliton, on wavelength separation has also been determined. FIGURE 4.6 shows that when using a Gaussian pulse with the same input peak power of the N=2 soliton, a reduced wavelength separation results. The amount of this decrease is less than 10 percent of the maximum wavelength separation.

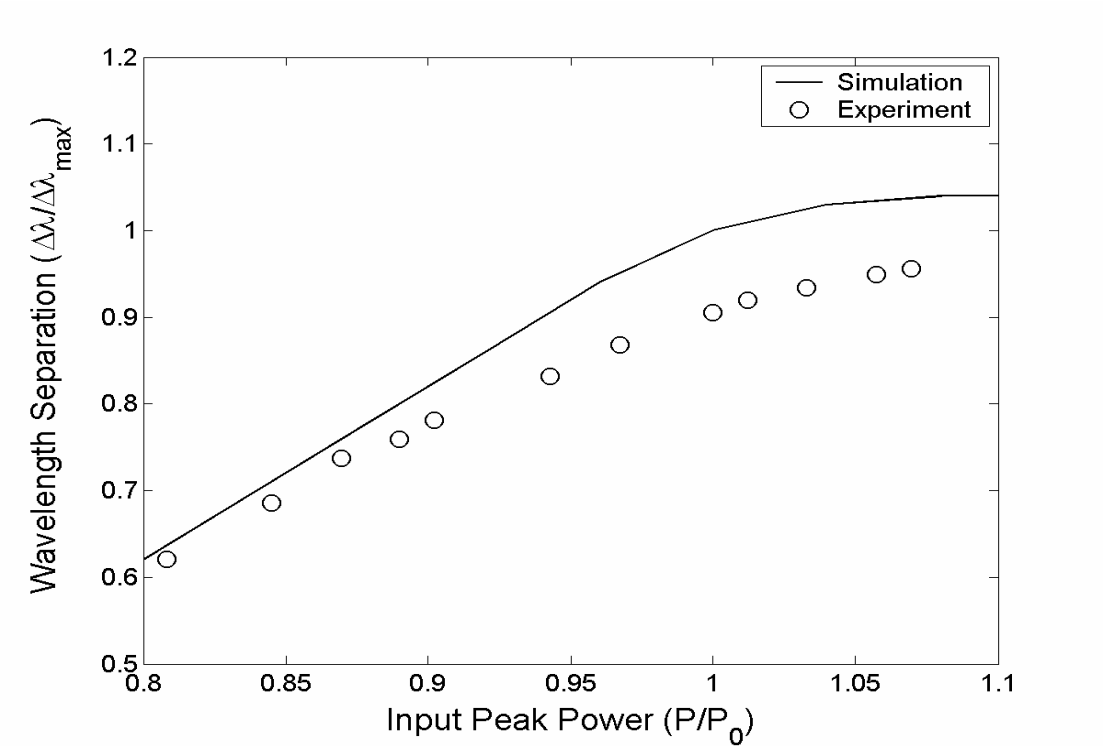

FIGURE 4.4 Measured and simulated wavelength separation to input power fluctuations in the fiber channel.

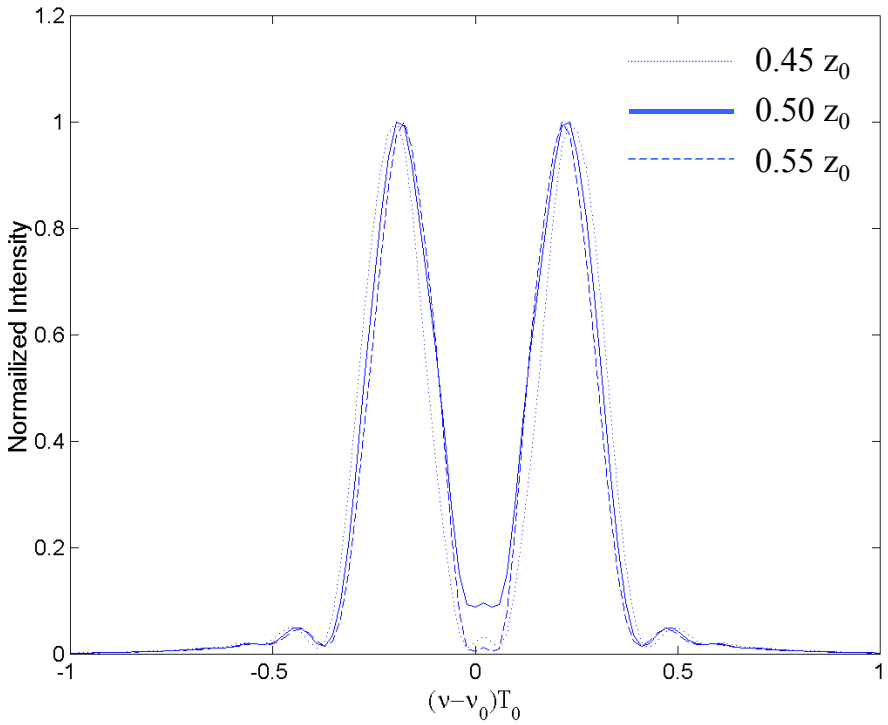

FIGURE 4.5 Output spectra obtained when changing the perturbation location from the maximum wavelength separation location (0.50 z_0) to 0.45 and 0.55 z_0.

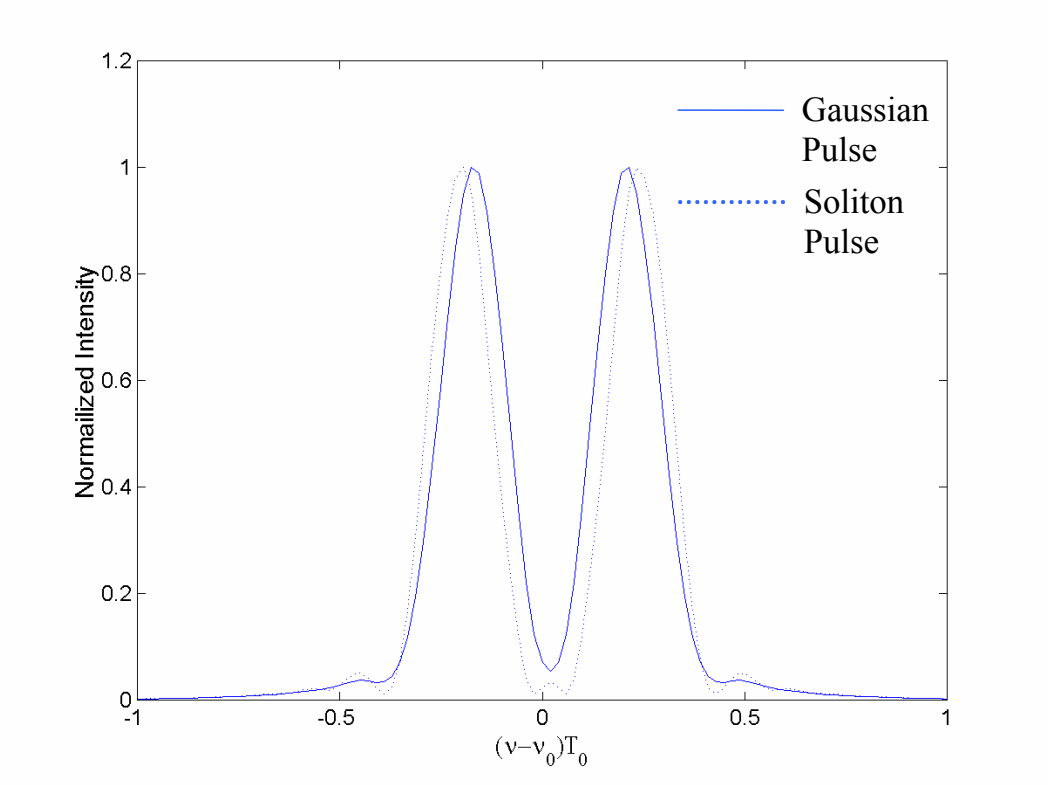

FIGURE 4.6 The effect of using a non-soliton pulse (Gaussian pulse) on wavelength separation.

4.4 Experiments Using a Loss Element

In this section, we experimentally demonstrate a tunable wavelength conversion using N=2 soliton decay initiated by a loss element. Figure 4.7 shows the experimental setup. F8L is used to produce a 1-ps FWHM soliton pulse. The output from a F8L was amplified by an EDFA and then launched at location A such that its pulse width and intensity satisfied the N=2 soliton condition within the LDF section. The center wavelength was 1560 nm and the peak power was 36 W. To introduce a loss perturbation, a variable attenuator is used between a half soliton period of an LDF and two soliton periods of an LDF, whose dispersion parameter at 1550 nm is 4.3 ps/km/nm and mode field diameter (MFD) is 8.4 μm. The variable attenuator drops the pulse peak power and reduces the value of N. After the loss perturbation, N=2 soliton decays forming two subpulses at the separate wavelengths.

Output spectrum measurements at location C are shown in Figure 4.8. By changing the amount of attenuation, wavelength separations between two subpulses are measured. Wavelength separations between 3nm and 5 nm are obtained for the attenuations between 3 dB to 8 dB.

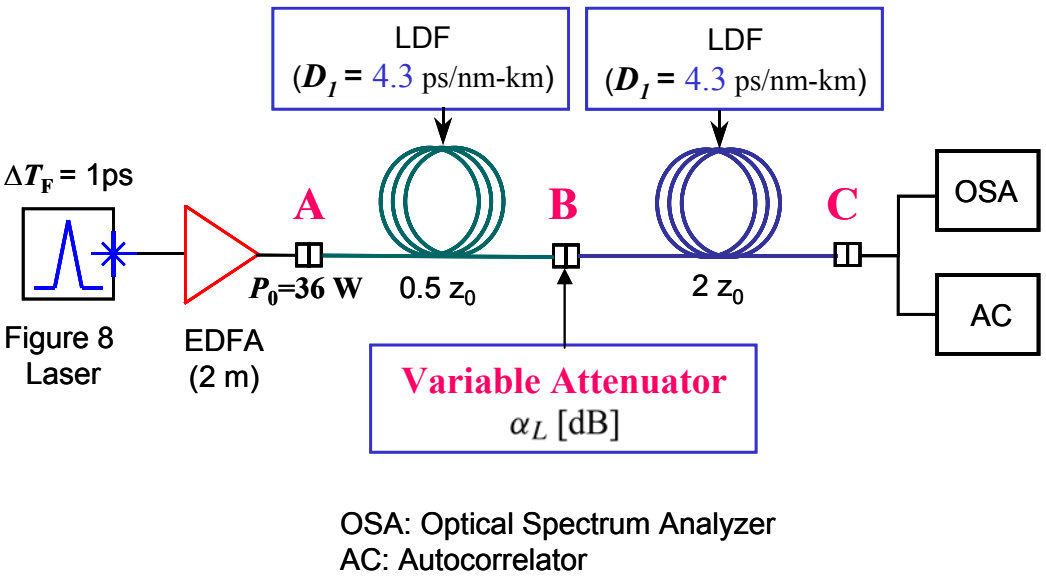

FIGURE 4.7 Experimental setup for N=2 soliton decay using a loss element; OSA: Optical Spectrum Analyzer and AC: Auto-Correlator.

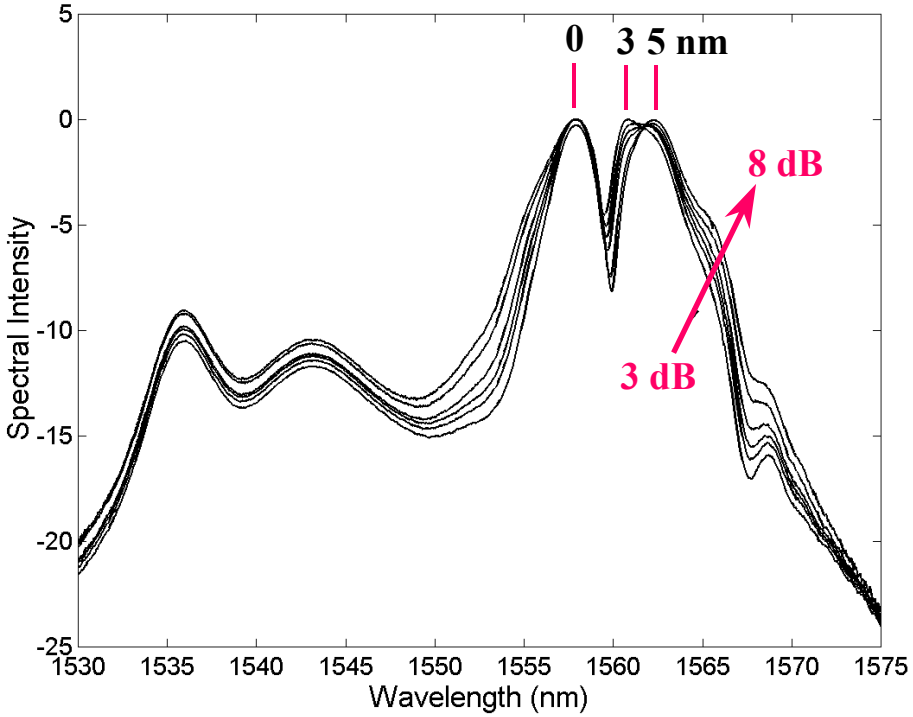

FIGURE 4.8 Output spectral separations achieved using a variable attenuator. Wavelength separations between 3~5 nm are obtained by changing the attenuation from 3~8 dB.

CHAPTER 5

SOLITON RECOVERY

5.1 Introduction

In the previous chapters, we have proposed and demonstrated the decay of higher order solitons in optical fiber, initiated by a step change in dispersion or by a localized loss element or filter as a means of generating pairs of pulses having wavelengths that are up and down-shifted from the input wavelength. After the soliton decay, recovery of the soliton by applying a reverse perturbation down-channel was also found to be feasible, provided that dispersion in the channel between perturbations is compensated and that higher order dispersion and nonlinearities are low. In this chapter, the possibility of recovering the original higher-order soliton by using appropriate perturbing elements, along with dispersion compensation will be studied. The conditions are described under which the separated pulses can be re-combined at a distant location to restore the higher order soliton at the original wavelength. Numerical and experimental studies for soliton recovery will be performed.

5.2 Conditions for Soliton Recovery

It is possible to recombine the two pulses and thus restore the original higher order soliton at a point farther down the channel. The requirements for this to occur are stringent, since the pulse widths, phase, and separation that occurred at the perturbation must be reproduced at the point of recombination. This ideally requires that the sub-pulses undergo completely linear propagation with no losses after the perturbation, and that dispersion and walk-off are precisely compensated. We show later that some deviation from the ideal is allowed. By incorporating a sufficiently large perturbation (a large dispersion increase, for example), the nonlinear response can be reduced sufficiently so that subsequent pulse propagation occurs essentially in the linear regime. In such cases, the separated pulses broaden and eventually dissipate due to group dispersion, but can nevertheless remain intact over several soliton periods. By simultaneously compensating both the dispersive broadening and walkoff between the two pulses, it is feasible to reproduce, at a remote location in the channel, the phase structure and spacing between pulses that were found just after the perturbation. Then, by applying a perturbation that reverses the effect of the initial one (using an amplifier instead of a loss element, or stepping back down to the original dispersion, for example), the original higher-order soliton can in principle be recovered.

This above "mirror-imaging" process essentially involves a solution of the NLSE from the original output to the input, while reversing the sign of the dispersion, and incorporating the reverse perturbation. The basic requirements ideally include 1) a lossless linear channel between perturbation elements in which group dispersion and

walk-off are precisely compensated, and 2) perturbations that impart no additional phase structure onto the pulses. The first requirement is most easily satisfied if the dispersion in the channel segments between perturbations is purely quadratic – in which case a compensating section whose dispersion-length product is equal and of opposite sign to that of the first section can be employed. Higher order dispersion terms represent a degradation, and must be minimized. A step in dispersion, either upward or downward, would meet the second requirement, whereas a bandpass filter or a loss element (requiring an amplifier as a restoring perturbation) would in general not.

5.3 Experiments on Soliton Recovery

Figure 5.1 shows the experimental setup for soliton recovery. To compensate the dispersion, we used 9 m of dispersion compensation fiber (DCF) having a dispersion of –91 ps/km-nm. The total dispersion at the second stage must be compensated by the total dispersion at the third stage. Thus, the requirement to do this is $z_2 \times D_2 = -z_3 \times D_3$.

In the experiment, the 1-ps FWHM output from the F8L was amplified by the EDFA and then launched at location A as before such that its pulse width and intensity satisfied the N=2 soliton condition within the initial LDF section. The fiber parameters and lengths for the segment between locations A and C are the exactly same as those in the previous experimental setup for the soliton decay shown in Figure 4.1.

The segment between locations C and D is dispersion-compensating fiber (DCF), having D_3 = -91 ps/nm-km. The purpose of this segment is to equalize the quadratic dispersion and sub-pulse walkoff that occur in the SMF-28 section. Finally, the dispersion is stepped back to the original 4.3 ps/nm-km value at location D by connecting a second section of the LDF. With zero net dispersion between B and D, and with no losses, the pulse should ideally return to the amplitude and phase configuration that it had just before the first dispersion step at B. Beyond D, the pulse propagated through an additional distance of $4.5z_0$ in the low dispersion fiber, to location E, where measurements were again made. Ideally, recovery of the original input at A is expected at E, which in fact was observed.

Autocorrelation traces and spectral measurements at each stage (from A to E) are shown in Figure 5.2, along with results of the numerical simulations. Measurements at

location B confirm the expected N=2 soliton temporal compression and 6-nm spectral separation at the $z_0/2$ location. The increase in dispersion to 17 ps/nm-km at B lowers the effective nonlinear response (by significantly reducing the value of N) in the B-C segment. This allows the two sub-pulses to temporally separate and dispersively broaden, as was confirmed by the autocorrelation measurement at C. These results were found to be in excellent agreement with numerical simulations, shown as the dashed traces in Fig. 2. The dispersion-compensating section is observed to have re-compressed and restored overlap of the sub-pulses at location D. Finally, the autocorrelation trace of the pulse at location E resembles that of the original input. The spectrum at E differs from that of the input, but shows that most of the energy is re-centered on the original carrier. Our numerical model confirmed that incomplete recovery arises from the 2-dB insertion loss of the DCF and the residual nonlinear response between locations B and C. The shape of the recovered spectrum at E is extremely sensitive to the power and phase conditions at D. This sensitivity is demonstrated by the noticeable differences between the simulated and experimental spectra shown at E in Figure 5.2, which arise from only slight differences in those shown at D.

Residual SPM in the channel between positions B and D may also degrade the soliton recovery process by preventing the re-assembly of sub-pulse phases necessary to continue the original N=2 evolution from position D. Instead, incomplete evolution occurs, which leads to some residual power in the separated wavelengths. As you can see next section, simulations show that the spectral energy remaining near each sub-pulse wavelength after recovery increases as the residual SPM increases [6], leading to

increased distortion in the recovered pulse. The process is nevertheless tolerant of appreciable SPM between perturbations, in that most of the pulse energy is restored to the original center wavelength, as shown at location E in Figure 5.2.

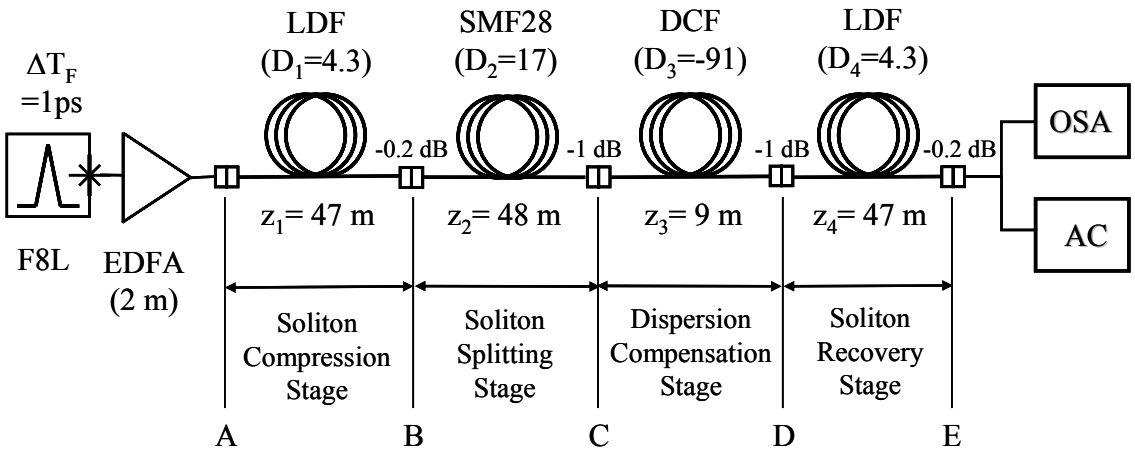

FIGURE 5.1 Experimental apparatus for demonstrating *N*=2 soliton decay and recovery. Pulsed input at A is provided by a figure 8 laser (F8L), amplified by a 2-m-long erbium-doped fiber amplifier (EDFA). Propagation segments include low-dispersion fiber (LDF), Corning SMF-28 fiber, and dispersion-compensating fiber (DCF). Pulse autocorrelation (AC) and spectral (OSA) measurements were made at each interface between stages (A through E). Splice losses are indicated at each interface. Dispersion values are in ps/nm-km.

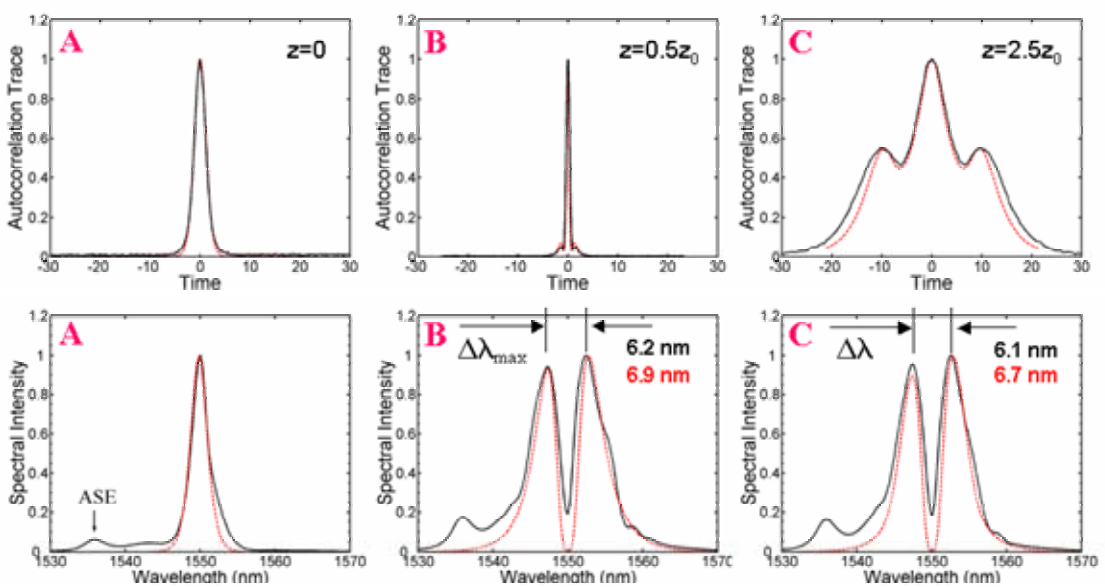

FIGURE 5.2 Measured (solid line) and simulated (dashed line) autocorrelation traces and spectra at locations A through E in the apparatus of Fig. 1. ASE is amplified spontaneous emission from the fiber amplifier.

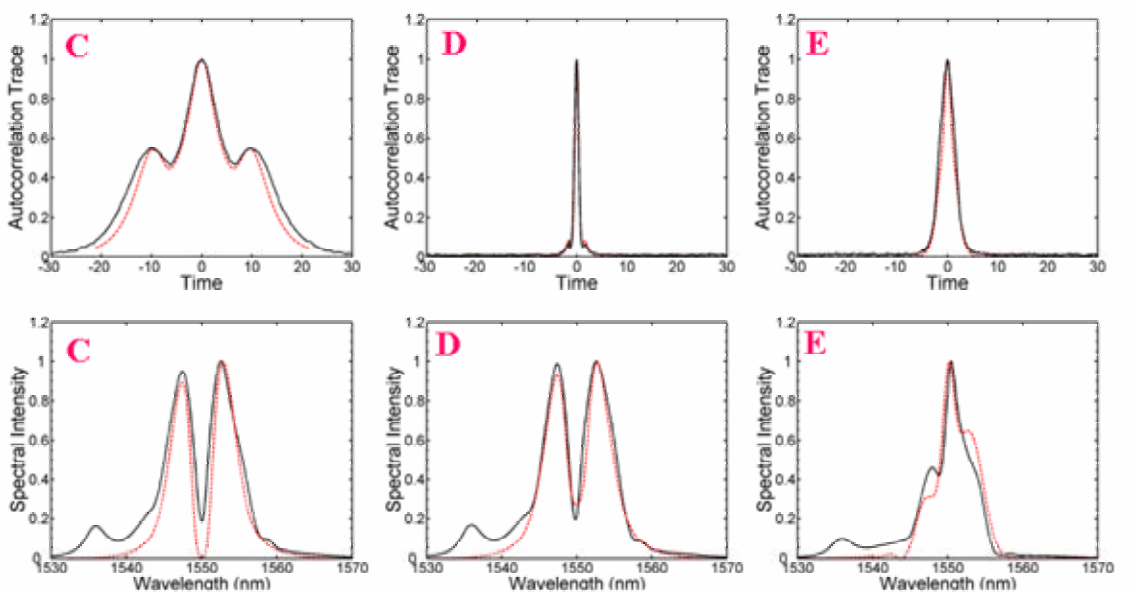

FIGURE 5.2 (continued)

5.4 Detrimental Effects on Soliton Recovery

In modeling the soliton recovery process, it was found that a small amount of cubic dispersion and even some residual nonlinearity in the channel between dispersion step perturbations can be present, without substantial degradation. Figure 5.3 shows N=2 pulse shapes and spectra after propagating through an initial step up in dispersion, followed by two channel segments having equal and opposite dispersion-length products, and finally a step down in dispersion to the original value. The initial dispersion step is adjusted to yield values of N in the intermediate channel (relative to the initial pulse width) of 1, $1/\sqrt{2}$, 1/2, and 0. As expected, the amount of distortion in the final recovered pulse is seen to increase as N increases. The process is nevertheless tolerant of appreciable nonlinearity between the perturbations, in that most of the pulse energy is restored to the original center wavelength in all cases shown.

Studies were also made of the allowed tolerances in achieving wavelength separation and soliton recovery. Of particular concern are the effects of power fluctuations in the input, losses in the propagation path, and low-level self phase modulation (SPM) in the dispersion-compensated link. We determined that the input pulse does not need to precisely satisfy the N=2 soliton condition in order to achieve a cleanly divided spectrum, but that the separation at a fixed location decreases as a nearly linear function of decreasing input power. Specifically, a power decrease by a given percentage results in approximately twice that percentage decrease in spectral separation. Increasing the input power beyond the N=2 condition slightly increases the spectral

separation, which eventually saturates to a maximum, while a third peak begins to form at the original carrier wavelength.

Splice loss and distributed fiber loss can decrease the spectral separation of the sub-pulses by diminishing the power during propagation. The effect of distributed loss (typically 0.2 dB/km) is negligible for short (~ 1 ps) pulses. With longer pulses, a longer fiber path is needed (because the soliton period increases) so that losses can have appreciable effect. To achieve the maximum spectral separation with losses present, an added length of LDF is required. For example, using a 10-ps input pulse, a $0.55z_0$ length is needed instead of $0.5z_0$ if the loss is 0.2 dB/km. After sub-pulse formation, the effect of the fiber loss is the expected power reduction with distance, along with the eventual pulse dissipation. To achieve complete soliton recovery, the pulse energy must be maintained so that the N=2 condition is re-established at the second dispersion step.

FIGURE 5.4 shows the output spectral changes arising from insufficient dispersion and walkoff compensation. Cases are shown for values of 5 (solid), 3(dashed), and 0 % (dotted). Influence of stimulated Raman scattering on soliton recovery for a 1ps N=2 soliton is shown in Figure 5.5.

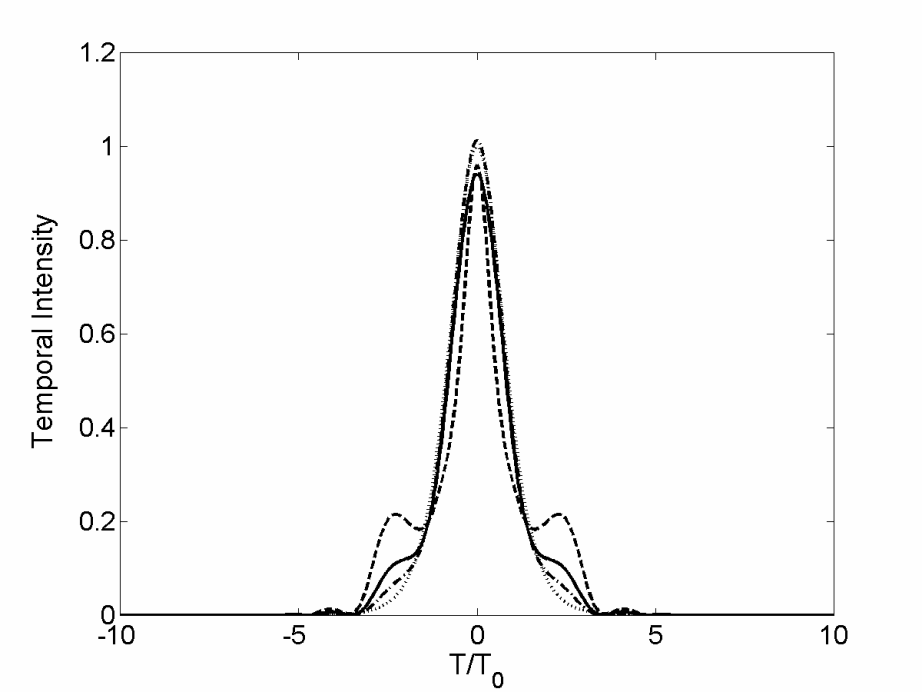

(a)

FIGURE 5.3 N=2 soliton pulse shapes (a) and spectra (b) after reverse-perturbation recovery as described in the text. Cases are shown for values of N between perturbations of 1 (dashed), $1/\sqrt{2}$ (solid), 1/2(dash-dotted), and 0 (dotted).

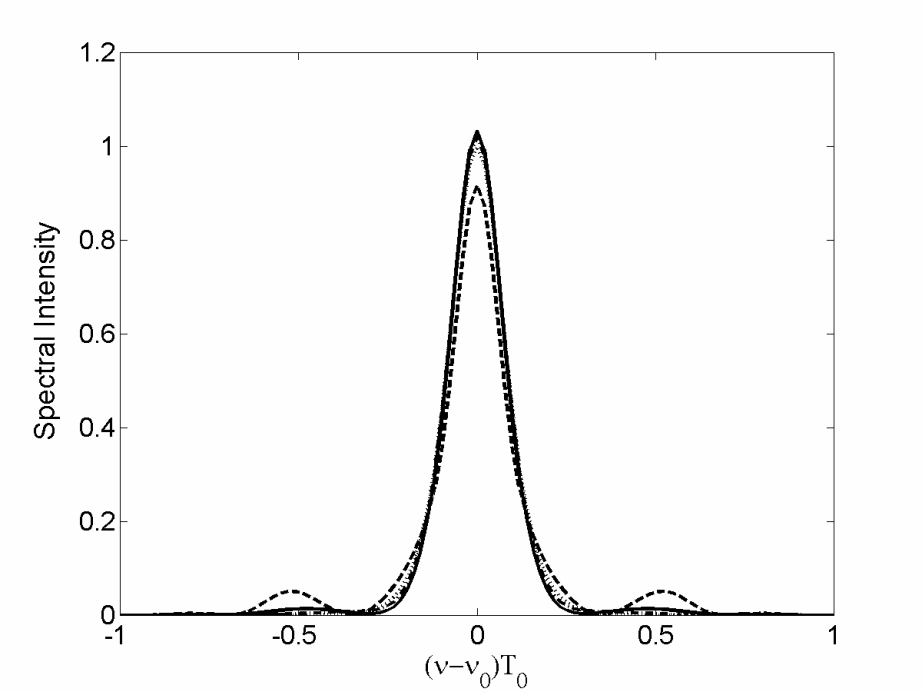

(b)

FIGURE 5.3 N=2 soliton pulse shapes (a) and spectra (b) after reverse-perturbation recovery as described in the text. Cases are shown for values of N between perturbations of 1 (dashed), $1/\sqrt{2}$ (solid), 1/2(dash-dotted), and 0 (dotted).

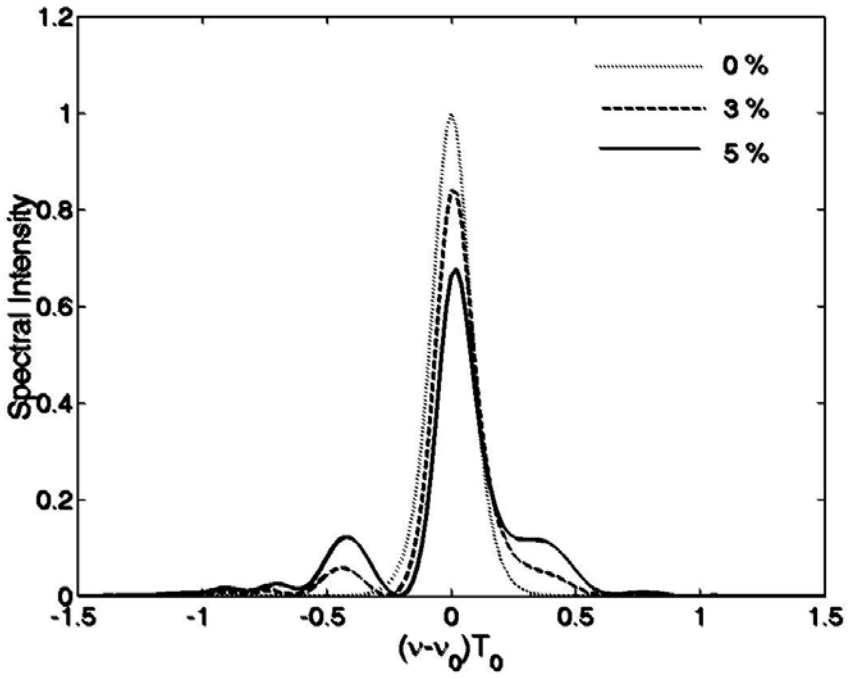

FIGURE 5.4 Output spectral changes arising from insufficient dispersion and walkoff compensation. Cases are shown for values of 5 (solid), 3(dashed), and 0 % (dotted).

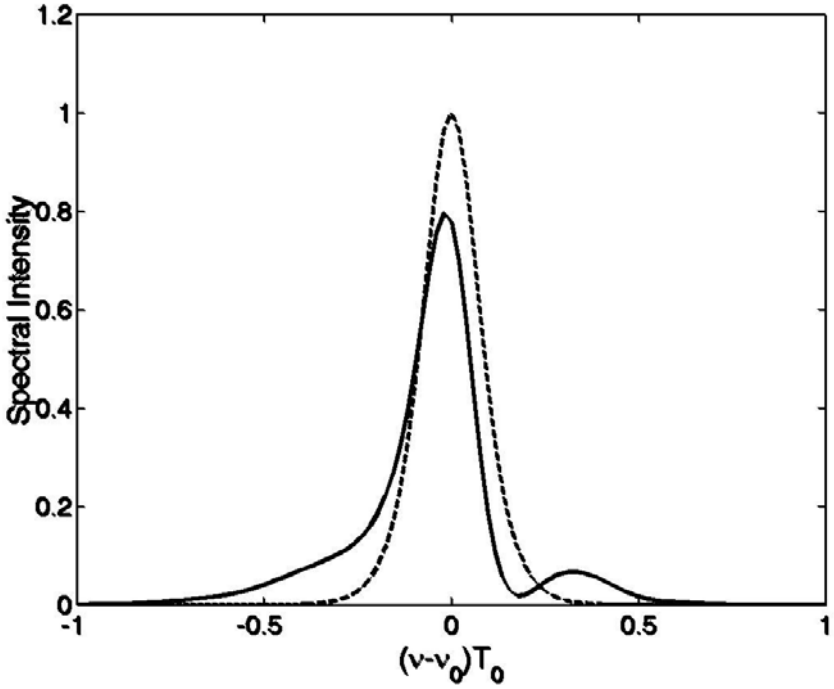

FIGURE 5.5 Influence of stimulated Raman scattering on soliton recovery

CHAPTER 6

PROPOSED APPLICATIONS

6.1 Introduction

The proposed applications can be grouped into two general categories:

1) the demonstration of data stream replication at several carrier wavelengths using cascaded loss element perturbations interleaved with optical amplifiers;

2) the demonstration of original data stream recovery from two wavelengths using a reverse perturbation. Accompanying the second category is the investigation of a proposed method of secure transmission that uses the phased re-assembly requirement for the N=2 solitons.

6.2 Multi-Wavelength Data Replication

In this work, the objective is to demonstrate the generation of a comb of wavelengths from a single wavelength RZ data stream, using the N=2 soliton spectral division effect. FIGURE 6.1 shows the proposed experiment, designed to generate eight wavelengths using a three stage device. In it, the original data stream is amplified to a series of N=2 solitons, which are then reduced in power at their $z_0/2$ location by a variable loss element. Once the wavelength-separated pulse trains complete the partial re-compression of their spectra, they are to be amplified and transmitted through a second lower-loss element. After spectral re-compression, the pulses are again spectrally divided, but the spacing between adjacent wavelengths is less. Re-amplifying and transmitting all four through a third loss element will then yield eight copies of the original data. By adjusting the loss element values, it should be possible to produce nearly equal wavelength spacing between the data replicas. Evolution of the data replicas into fundamental solitons is not anticipated in this experiment, since the loss elements remove sufficient energy from the sub-pulses so that the N=1 condition cannot be satisfied [10]. Use of dispersion steps would in principle allow this; we intend to attempt such a study provided fiber of the correct dispersion can be located. Studies are to be made of the effects of accumulated amplifier noise, and an assessment is to be made of the maximum number of stages that can be practically employed before noise and other degrading effects limit performance.

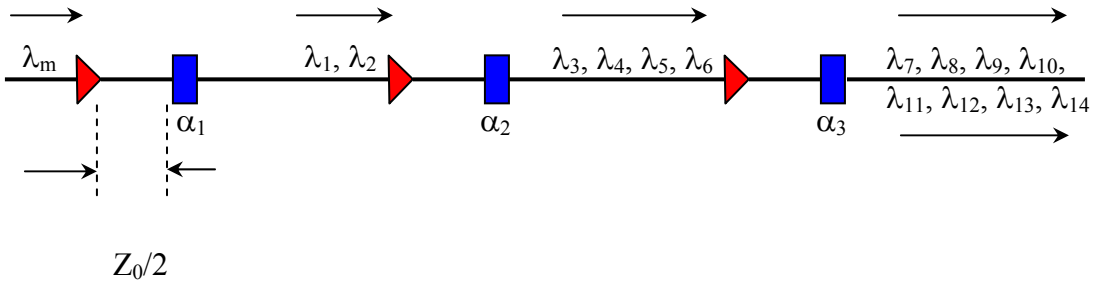

FIGURE 6.1 Scheme for multi-wavelength replication of a data stream at wavelength λ_m by using cascaded amplifier-loss element pairs. The distance between each amplifier and loss element is one-half the soliton period.

6.2 Secure Data Transmission

In this portion of the work, a method of establishing secure data transmission is to be explored that uses the phase-sensitive properties of soliton recovery. The basic diagram for the scheme is shown in Figure 6.2. In the figure, a single wavelength data stream is input at the left, amplified, and N=2 solitons are allowed to form. At a point just before the first perturbation, a step up in dispersion, the spectrum has separated, and the dispersion step initiates the temporal separation between the two data streams as described previously. Both data sets are then sent through a phase modulator which imparts a digital code (in this case 10101) onto the otherwise uniformly spaced pulses. The pulses that were acted upon by the modulator have had their phasing disrupted, and so will not recombine at the original wavelength. At the output, one thus obtains the inverse of the data stream at the restored carrier wavelength, and the data as imparted by the modulator appears on the two wavelength-shifted components. Without back-conversion, only a continuous sequence of "one" bits is received at the two shifted wavelengths.

The scheme is potentially attractive because it is not possible to recover the data at any point in the channel other than at the receiver end, at which complete dispersion compensation has occurred. This allows the pulses that have not been modulated to combine, return to the original center wavelength, and be direct detected as the message imparted by the modulator. This can happen nowhere else in the channel.

Proposed efforts on this system will initially involve studies of the effect on the pulses of phase modulation. It is anticipated that the modulation when applied to pulses at

different wavelengths will disrupt their relative phasing to an extent that is sufficient to prevent their re-assembly into the original pulse at the center wavelength. Otherwise, it is possible to let the pulses separate temporally such that they have negligible overlap upon reaching the modulator. A fast modulator can then be used to affect a pulse at one wavelength, but not the adjacent one at the other wavelength. Figure 6.3 shows apparatus for demonstrating secure data transmission using the phase-sensitive properties of soliton recovery. A phase modulator is inserted between SMF28 and DCF in the previous soliton recovery setup shown in Figure 5.1. Figure 6.4a shows that the pulse shape before phase modulation and the profiles of phase modulation. The modulation is applied to the one side of the subpulse with 0, $\pi/3$, and π phase difference. Simulation results for the N=2 soliton pulse shapes and spectra after phase modulation and reverse-perturbation recovery are shown in Figure 6.4b and 6.4c. The pulse modulated with 0 phase modulation returns to the original center wavelength whereas the pulse with π phase modulation shows complete spectral separation. The pulse with $\pi/3$ phase modulation has not much spectral change comparing to the case of 0 phase modulation. To get a sufficient change in spectrum, the modulator needs to be operated near π phase modulation.

Figure 6.5 shows an experimental setup for the secure data transmission using the phase-sensitive properties of soliton recovery. The total system loss is -9.2 dB including the -5.6 dB insertion loss of the phase modulator. This added loss prevents the subpulse from recombining at the original center wavelength even when 0 phase modulation is used. One method to overcome this problem is to use a different LDF, which has a less dispersion parameter, at the last stage of the experimental setup. From Equation (2.2.7),

further decrease in D may be used to compensate added loss (or reduction of P_0), when restoring N = 2. For -9.2 dB loss, the required dispersion is 0.51 ps/km-nm. In our experiment, half soliton period of LDF with dispersion parameter of 0.54 ps/km-nm is used to overcome the loss. Figure 6.6 shows the measured and simulated spectrum after phase modulation and reverse-perturbation recovery. After 0 phase modulation, the spectrum is recovered at the original center wavelength.

The rising time of the phase modulator is 35 ps, which is too slow to modulated only one side of subpulse as shown in Figure 6.4. We need a faster phase modulator. One alternative method to solve this problem is to use longer SMF28 and DCF to introduce enough separation between to subpulses. When we use 20 z_0 of SMF28, we can obtain about 100 ps separation for a 1ps input pulse. However, the total system loss increases to -11 dB to increase the length of SMF28 and DCF. This requires 0.34 ps/km-nm LDF at the last stage in the experimental setup, which we have not now.

For the recommended future researches, studies need to be performed on the robustness of the link, with regard to quantifying low-level nonlinear responses in the channel section between perturbations that will still allow pulse recovery at the receiver end. Additionally, effects of cubic dispersion and stimulated Raman scattering in the intermediate channel need to be investigated.

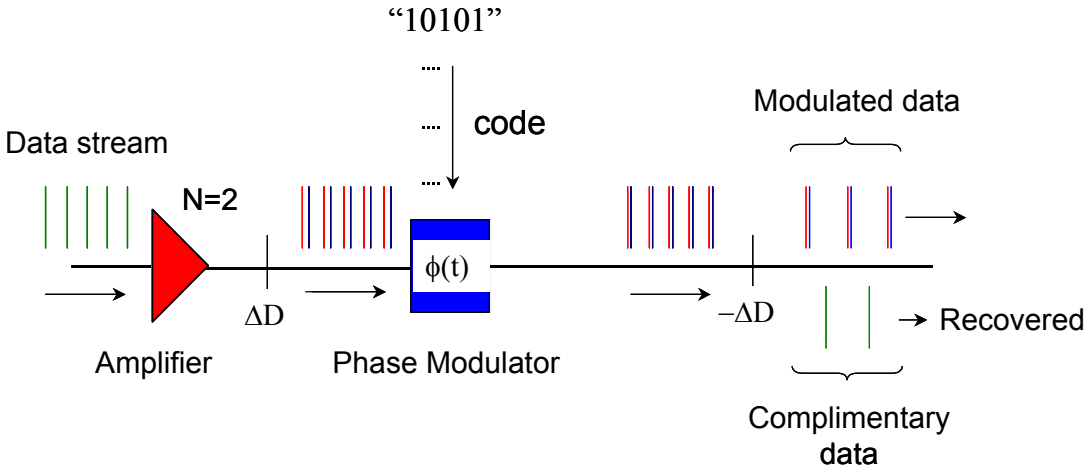

FIGURE 6.2 Basic soliton recovery link employing dispersion step perturbations, and phase modulation to code the data stream. The portion of the link between perturbations is dispersion compensated and requires linear propagation.

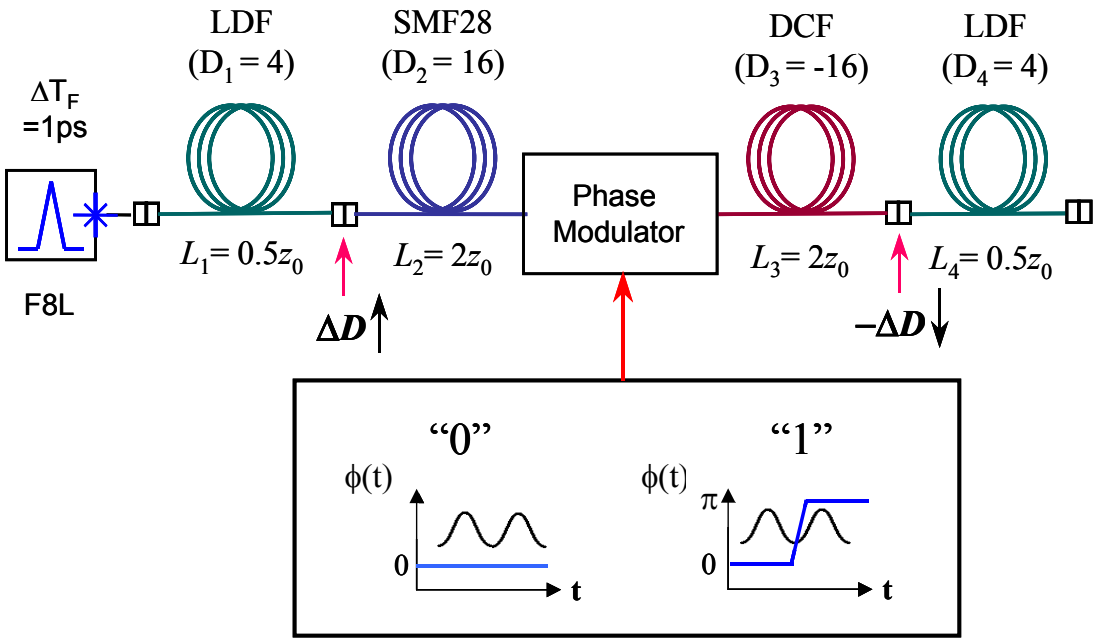

FIGURE 6.3 Apparatus for secure data transmission using the phase-sensitive properties of soliton recovery

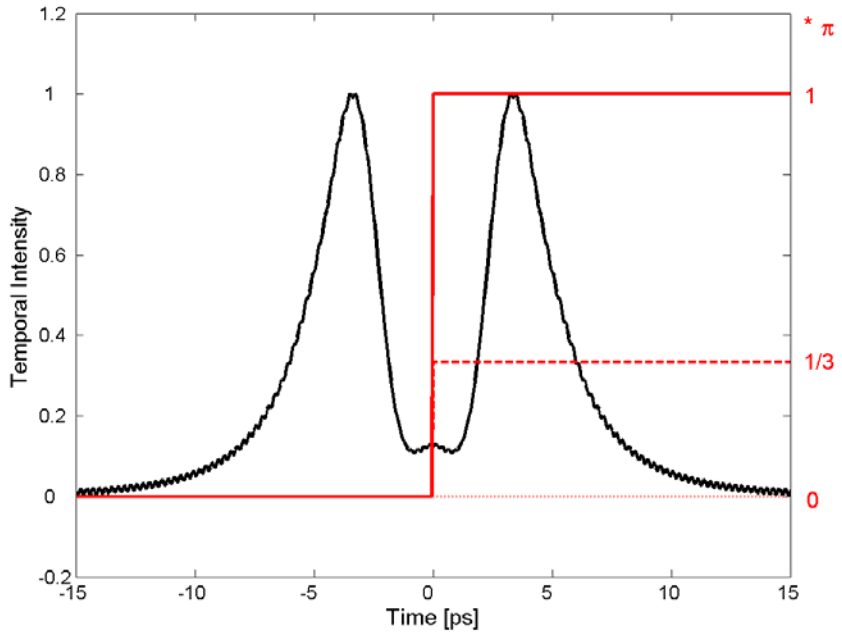

(a)

FIGURE 6.4a Pulse shapes before phase modulation. "0" (dotted), "π/3" (dashed), and "π" (solid) phase modulations are applied to the pulse.

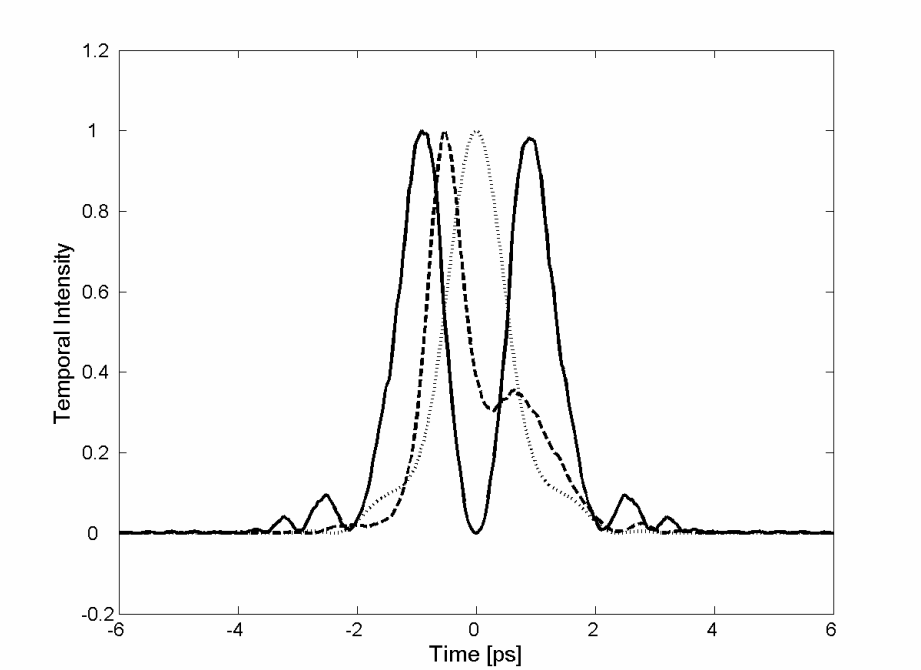

(b)

FIGURE 6.4b N=2 soliton pulse shapes after phase modulation and reverse-perturbation recovery. Cases are shown for "0" (dotted), "π/3" (dashed), and "π" (solid) phase modulations.

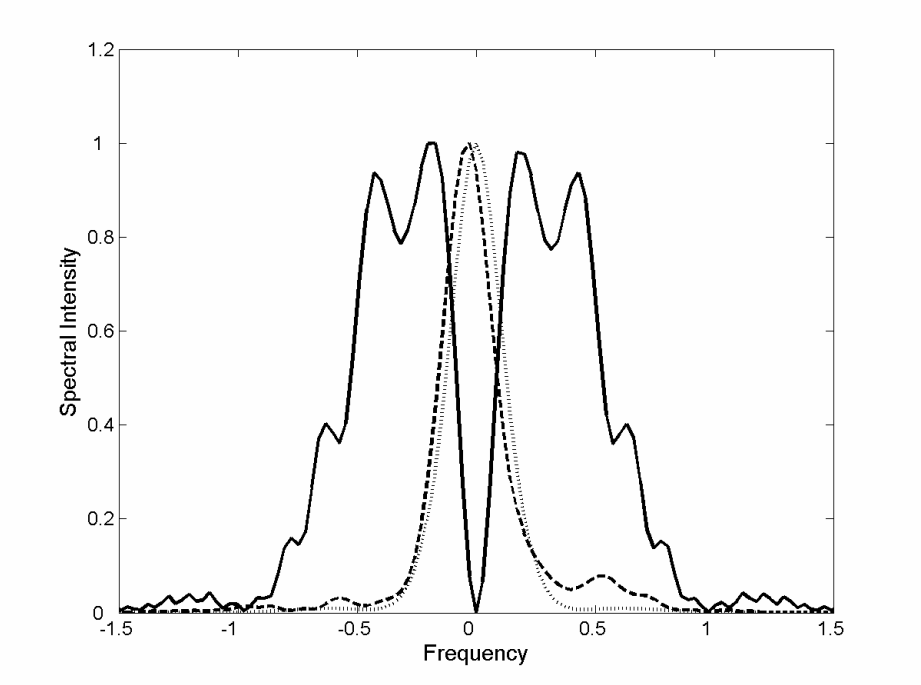

(c)

FIGURE 6.4c N=2 soliton pulse spectra after phase modulation and reverse-perturbation recovery. Cases are shown for "0" (dotted), "π/3" (dashed), and "π" (solid) phase modulations.

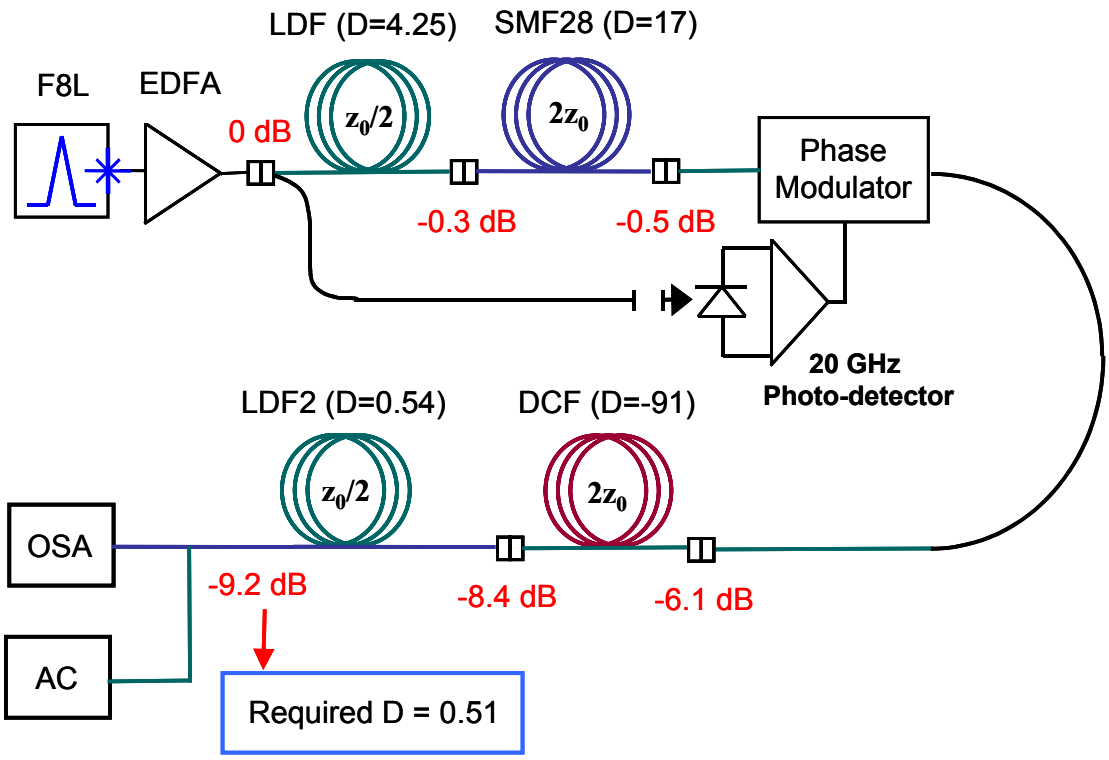

FIGURE 6.5 Experimental setup for the secure data transmission using the phase-sensitive properties of soliton recovery.

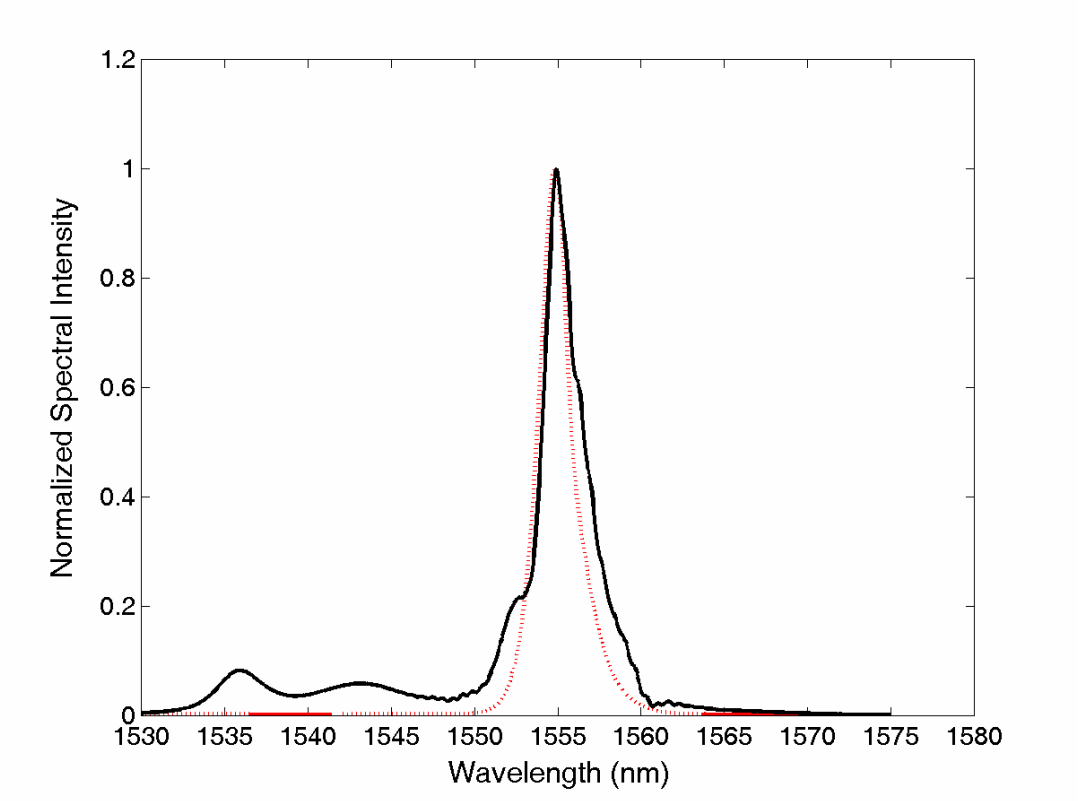

FIGURE 6.6 Measured (solid) and simulated (doted) spectrum after phase modulation and reverse-perturbation recovery for 0 phase modulation.

CHAPTER 7

CONCLUSION

The object of this research was to investigate the decay and recovery of higher-order solitons initiated by localized channel perturbation. A detailed modeling effort for soliton propagation in optical fibers was performed to accomplish this task. A simulation tool was developed using split step Fourier method (SSFM). The higher-order soliton decay initiated by a localized channel perturbation in the fiber channel has been demonstrated theoretically and experimentally as a means of generating pairs of pulses having wavelengths that are up and down-shifted from the input wavelength. Other effects such as Raman scattering and cubic dispersion were shown to de-stabilize the process, but can be minimized by operating with pulse widths on the order of 1 ps or longer. Recovery of the original pulse by applying a reverse perturbation down-channel was also found to be feasible, provided dispersion in the channel between perturbations is compensated, and that higher order dispersion and nonlinearities are low. The separated pulses at two wavelengths can in principle be amplified to form separate higher order solitons. The process is repeated to produce multiple wavelength replicas of an input data stream, and may thus be of possible use in multi-casting applications in fiber communication systems.

We have shown that the spectral separation effect in N=2 solitons can be used as a

method of converting a single pulse into two sub-pulses at displaced wavelengths by incorporating a dispersion step at the half soliton period location. Wavelength shifts are tunable by varying the magnitude of the dispersion step, or by varying the input pulse power above or below that required for the N=2 soliton condition. The method may find applications in WDM data transmission, in that two wavelength-converted replicas of a single data stream can be generated. Proposed applications have been presented for the wavelength separation and recovery processes.

References

[1] E. A. Golovchenko, E. M. Dianov, A. M. Prokhorov, and V. N. Serkin, “Decay of optical solitons,” JETP Lett. 42, 87-91, 1985.

[2] K.Ohkuma, Y.H. Ichikawa, and Y.Abe, “Soliton propagation along optical fibers”, Opt. Lett., 12, 516-518, 1987.

[3] Kuochou Tai and Akira Hasegawa, “Fission of optical solitons induced by stimulated Raman effect”, Opt. Lett. 13, 392-394, 1988.

[4] P. K. Wai, C. R. Menyuk, Y. C. Lee, and H. H. Chen, “Nonlinear pulse propagation in the neighborhood of the zero-dispersion wavelength of monomode optical fibers”, Opt. Lett. 11, 464-466, 1986.

[5] S.R. Clarke, R.H.J. Grimshaw, and B.A. Malomed, “Soliton formation from a pulse passing the zero dispersion point in a nonlinear Schödinger equation”, Phys. Rev. E 61, 5794-5801, 2000.

[6] K.-S. Lee, M.C. Gross, S.E. Ralph, and J.A. Buck, "Wavelength conversion using N=2 soliton decay and recovery in fiber, initiated by dispersion steps", IEEE Photonics Technol. Lett., vol. 16, no. 2, 2004.

[7] K.-S. Lee and J. A. Buck, "Wavelength conversion through higher-order soliton splitting initiated by localized channel perturbations", J. Opt. Soc. Am. B, vol. 20, no. 3, 2003.

[8] V. E. Zakharov and A. B. Shabat, “Exact theory of two-dimensional self-focusing and one-dimensional self-modulation of waves in nonlinear media,“ Sov. Phys. JETP 34, pp 62-70, 1972.

[9] J. Satsuma and N. Yajima, “Initial value problem of one-dimensional self-modulation of nonlinear waves in dispersive media,” Prog. Phys. Suppl. 55, pp. 284-300, 1974.

[10] C.R. Menyuk, “Soliton robustness in optical fibers”, J. Opt. Soc. Am. B 10, 1585-1591, 1993.

[11] W. Hodel, and H.P. Weber, “Decay of femtosecond higher-order solitons in an optical fiber induced by Raman self-pumping”, Optics Lett., 12 924-926, 1987.

[12] John A. Buck, Fundamentals of Optical Fibers, Wiley Interscience, New York, 1995.

[13] E. Bourkoff, W. Zhao, R. I. Joseph, and D. N. Christodoulides, Opt. Lett. 12, 272, 1988.

[14] E. A. Golovchenko, E. M. Dianov, A. N. Pilipetskii, A. M. Prokhorov, and V. N. Serkin, JETP Lett. 45, 91, 1987.

[15] F. DeMartini, C. H. Townes, T. K. Gustafson, and P. L. Kelley, Phys. Rev. 164, 312, 1967.

[16] J. T. Manassah, M. A. Mustafa, R. A. Alfano, and P. P. Ho, IEEE J. Quantum Electron. QE-22, 197, 1986.

[17] P. Beaud, W. Hodel, B. Zysset, and H. P. Weber, IEEE J. Quantum Electron. QE-23, 1938, 1987.

[18] A.K. Atieh, P. Myslinski, J. Chrostowski, and P. Galko, “Measuring the Raman time constant for soliton pulses in standard single-mode fiber”, J. Lightwave Tech., 17, 216-221, 1999.

[19] G.P. Agrawal, *Nonlinear Fiber Optics, 3rd ed*, Academic Press, San Diego, 2001.

[20] M. Nakazawa, H. Kubota, and K. Tamura, “Random evolution and coherence degradation of a high-order optical soliton train in the presence of noise”, Opt. Lett. 24, 318-320, 1999.

[21] P.L. François, “Nonlinear propagation of ultrashort pulses in optical fibers: total field formulation in the frequency domain”, J. Opt. Soc. Am. B, 8, 276-293, 1991.

Appendix

SSFM Programming using MATLAB for Nonlinear Pulse Propagation in Optical Fibers

1. Definition of Parameters

First thing we need to do in the beginning stage of programming is to define parameters. Determine input parameters (such as input pulse width and peak power) and fiber parameters (such as dispersion parameter, nonlinear coefficient, and Raman response parameter in an optical fiber).

Then we need to set programming parameters and constants. The step size is an important programming parameter because it is a major factor to determine the numerical error of the SSFM. An assumption of the SSFM is to calculate linear terms and nonlinear terms in the NLSE independently in a small segment. To satisfy this assumption, we need enough resolution for the step size. If we decrease it, the error will be reduced whereas the calculation time increases. As the step size deceases, the numerical result converges. The efficient way to set the step size is to use 10~20 times smaller step size than the step size, which gives the permitted error.

If we use a too small step size, the number of computation increases. This increases the numerical error from computational operation. However, we can get enough accuracy before this error becomes critical.

```
% Examples of Input Parameters

lambda=1.55*10^(-6);   % operating wavelength in micrometer
Wo=2*pi*c/lambda;      % angular frrequency
pulsewidth=1;          % input pulse width in ps
Po= 36;                % input peak power
Ao=sqrt(Po);           % input peak amplitude


% Examples of Fiber Parameters

b2=-5;             %quadratic dispersion parameter  in ps^2/km
b3=0;              % cubic dispersion parameter  in ps^3/km
non_coeff=2;       % nonlinear  coefficient in /W/km
TR=3*10^(-15);     % Raman response parameter in second
shock=0;           % switch for optical shock (1:on 0:off)
loss_fiber=0;      % fiber loss in dB
alpha=log(10)*loss_fiber/10;



% Examples of Programming Parameters and Constants

PI=3.14;   % π
N=1024;    % number of sample in time domain
M=100;     % number of step
To=20;     % characteristic pulse width of soliton
c=2.99*10^8; % speed of light in free space

z=0.5*soliton_length;              % propagation distance
step_size = z/M;                   % step size
sampling_time = pulsewidth/To;     % sampling time interval
```

2. Initialization

After defining all parameters, we initialize the input pulse shape and spectrum, and calculate the required parameters, which will be used in the next step.

```
% Example

Ld=(pulsewidth^2)/abs(b2);     % dispersion length
Lnl=1/(non_coeff*Po);          % nonlinear length
soliton_length=pi*Ld/2;        % soliton period
soliton_order=sqrt(Ld/Lnl);    % soliton order


% Define Input Pulse Shape

for n=1:N,

  u(n)= Ao*sech((n-N/2-1)/To);

end

spectrum=fft(u);       % Pulse spectrum
```

3. Implementation of Split Step Fourier Method

To implementing the SSFM, we use a loop structure to solve the NLSE step by step. All parameters are plug into the NLSE. As described in Section 2.3, under some assumption that dispersion and nonlinearity can act independently during the propagation of the optical field over a small distance, propagation from z to z+h is carried out in three steps. In the first step, only dispersion is considered for the first half of the segment. Then, only nonlinearity is considered in the middle of the segment. In the third step, only dispersion is considered again for the rest half of the segment.

```
% Example

for j=1:M,          % M: number of step
    % Calculation of Fiber Loss and Dispersion for the first half of a segment
    for k=1:N,
        spectrum(k) = spectrum(k) *
                      exp((-alpha/2 +(i*b2/2)*(2*PI*(k-N/2-1) /(pulsewidth/To)/N)^2
                     -i*b3/6*(2*PI*(k-N/2-1)/(pulsewidth/To)/N)^3)*z/M/2.0);
    end
    u=ifft(spectrum);          % Inverse Fourier transform

    % Calculation of nonlinearity at the midpotint of a segment
```

```
    for n=1:N,
        u(n)=u(n)*exp(i*non_coeff*((abs(u(n)))^2                    % SPM
                                   +i*shock*Steep(n)/Wo/e_f(n)      % Optical Shock
                                   -TR*Raman(n))*z/M);              % Raman
    end

    spectrum=fft(u);       % Fourier transform




    % Calculation of Fiber Loss and Dispersion for the rest half of a segment


    for k=1:N,

        spectrum(k) = spectrum(k) *
                        exp((-alpha/2 +(i*b2/2)*(2*PI*(k-N/2-1) /(pulsewidth/To)/N)^2
                       -i*b3/6*(2*PI*(k-N/2-1)/(pulsewidth/To)/N)^3)*z/M/2.0);
    end

    u=ifft(spectrum);           % Inverse Fourier transform


end
```

4. Self-Steepening and Raman Coefficients

Self-steepening parameters and stimulated Raman scattering response coefficients can be calculated and plugged into the above loop. For the pulse width greater than 1 ps, these effects can be ignored and the parameters can be set to zero.

```
Steep(1)=0;
Raman(1)=0;

for n=2:1:N-1,

    Steep(n)= (u(n+1)^2*u(n+1)-u(n-1)^2*u(n-1))/(2*pulsewidth*10^(-12)/To);
    Raman(n)=(u(n+1)^2-u(n-1))/(2*pulsewidth*10^(-12)/To);

end


Steep(1)=Steep(2);
Raman(1)=Raman(2);

Steep(N)=Steep(N-1);
Raman(N)=Raman(N-1);
```